Song H, Endow SA (1996) Binding sites on microtubules of kinesin motors of the same or opposite polarity. *Biochemistry* **35**: 11203–11209

Song H, Golovkin M, Reddy ASN, Endow SA (1997) *In vitro* motility of AtKCBP, a calmodulin-binding kinesin protein of *Arabidopsis*. *Proc Natl Acad Sci USA* **94**: 322–327

Studier FW, Rosenberg AH, Dunn JJ, Dubendorff JW (1990) Use of T7 RNA polymerase to direct expression of cloned genes. *Methods Enzymol* **185**: 60–89

Svoboda K, Block SM (1994) Force and velocity measured for single kinesin molecules. *Cell* **77**: 773–784

Svoboda K, Schmidt CF, Schnapp BJ, Block SM (1993) Direct observation of kinesin stepping by optical trapping interferometry. *Nature* **365**: 721–727

Visscher K, Schnitzer MJ, Block SM (1999) Single kinesin molecules studied with a molecular force clamp. *Nature* **400**: 184–189

©2004 European Molecular Biology Organization

nature
structural &
molecular biology

© 2005 Nature Publishing Group http://www.nature.com/nsmb

Motility of myosin V regulated by the dissociation of single calmodulin

HoaAnh Nguyen[1–3] & Hideo Higuchi[1,3]

Myosin V is a calmodulin-binding motor protein. The dissociation of single calmodulin molecules from individual myosin V molecules at 1 μM Ca^{2+} correlates with a reduction in sliding velocity in an *in vitro* motility assay. The dissociation of two calmodulin molecules at 5 μM Ca^{2+} correlates with a detachment of actin filaments from myosin V. To mimic the regulation of myosin V motility by Ca^{2+} in a cell, caged Ca^{2+} coupled with a UV flash system was used to produce Ca^{2+} transients. During the Ca^{2+} transient, myosin V goes through the functional cycle of reduced sliding velocity, actin detachment and reattachment followed by the recovery of the sliding velocity. These results indicate that myosin V motility is regulated by Ca^{2+} through a reduction in actin-binding affinity resulting from the dissociation of single calmodulin molecules.

Calcium regulates various enzyme reactions of cellular processes through direct interaction to modify the function of a protein or through indirect interaction with a Ca^{2+}-sensing protein. Among the Ca^{2+}-sensing proteins expressed in eukaryotic cells, calmodulin (CaM) is a member of the EF-hand family, and has been known to participate in many signaling pathways that affect crucial processes such as cell growth, proliferation and cell movement[1,2].

Myosin V is an unconventional double-headed myosin that transports synaptic and endoplasmic reticulum vesicles in neurons[3–5], pigment granules in melanocytes[6–8], and vacuoles in yeast[9,10]. Myosin V is a processive motor capable of taking 36-nm steps along actin filaments[11–13]. Structurally, myosin V is a homodimer. Each monomer has one N-terminal head domain, one extended neck domain that contains six IQ motifs, and a tail domain containing a coiled coil region attached to a C-terminal globular region[14–16]. The IQ motifs form binding sites for CaM and CaM-related light chains[14,16,17]. Recent studies have investigated whether CaM bound to the IQ motifs can regulate the function of myosin V in response to Ca^{2+} (refs. 16,18–21). Two of those studies have reported that myosin V stops moving but remains bound to actin filaments at high Ca^{2+} concentrations (>1 μM) in *in vitro* motility assays using nitrocellulose coated glass[19,20]. In this study, using an *in vitro* motility assay on uncoated glass slides, we observed the detachment of actin filaments from myosin V at high Ca^{2+} concentrations. This finding suggests that high Ca^{2+} concentrations are a novel way of inactivating the motility of myosin V. Furthermore, upon transient release of Ca^{2+}, myosin V reversibly detaches from and slides along actin filaments in the presence of free CaM. To provide insights into the underlying mechanism of this observation, we used single-molecule imaging to monitor the dissociation of individual CaM molecules from myosin V at various Ca^{2+} concentrations. Based on these observations, we propose a model explaining the regulation of the myosin V motor function resulting from the dissociation of single CaM molecules. This model shows how a motor protein detaches and then reattaches to their moving track. This may also explain how a multimotor-binding vesicle could be switched between different tracks for targeting in a cell.

RESULTS

Effect of Ca^{2+} on myosin V motility

To estimate the effect of Ca^{2+} on myosin V motility, we first developed a suitable glass surface for observing reversible motility in the *in vitro* assay (**Supplementary Methods** online). Using nitrocellulose-coated glass, movement was restored for only 56 ± 16% (mean values ± s.d., $n = 15$) of the actin filaments after removing Ca^{2+} in the solution. Using an uncoated glass surface, 96 ± 3% ($n = 15$) of the actin filaments showed movement. Thus, the remainder of our experiments were done using uncoated glass slides. The irreversible inactivation of myosin V on nitrocellulose-coated glass was most likely due to irreversible binding of myosin V molecules to the nitrocellulose at the hydrophobic site of IQ domains (containing ~40% hydrophobic residues)[15], which is exposed after the dissociation of CaM.

The *in vitro* motility assays for myosin V were done in the presence of various Ca^{2+} concentrations. At pCa 6.0, the number of sliding actin filaments was less than that in the absence of Ca^{2+} (pCa > 7.0). At pCa 5.6, all actin filaments detached from myosin (**Fig. 1a**). To analyze the effect of Ca^{2+} in detail, we quantified the number and velocity of actin filaments (**Fig. 1b,c**). In the absence of Ca^{2+} or at pCa 6.4, the density of sliding actin filaments was ~0.17 filaments μm^{-2}, and most of them (>95%) moved smoothly. However, at pCa 6.0 there was a large reduction in both the density of sliding filaments and velocity of sliding. At pCa 5.8, the velocity of a few actin filaments could still be observed. It was similar to that recorded at pCa 6.0 (~230 nm s^{-1}). Finally, at

[1]Center for Interdisciplinary Research, Tohoku University, Sendai 980-8578, Japan. [2]Laboratory of Applied Microbiology, Department of Molecular and Cell Biology, Division of Life Science, Graduate School of Agricultural Science, Tohoku University, Sendai 981-8555, Japan. [3]Biomedical Engineering Research Organization, Tohoku University, Sendai 980-8575, Japan. Correspondence should be addressed to H.H. (higuchi@material.tohoku.ac.jp).

Published online 23 January 2005; doi:10.1038/nsmb894

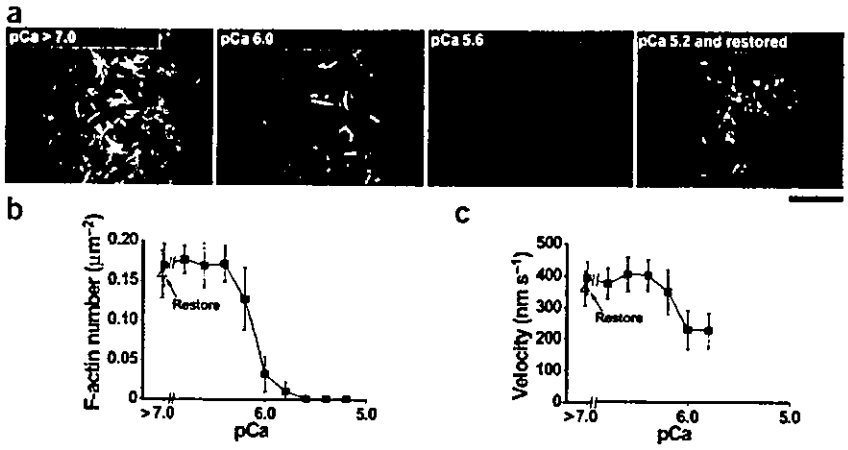

Figure 1 Effects of Ca^{2+} on the *in vitro* motility assay of myosin V. (**a**) *In vitro* motility assays carried out in the absence of Ca^{2+} (pCa > 7.0), and at pCa 6.0 and 5.6. At pCa 5.2, movement was restored by washing out Ca^{2+} in the presence of 10 μM CaM. Bar, 10 μm. (**b**,**c**) The number (**b**) and velocity (**c**) of sliding actin filaments (F-actin) at different pCa values in the *in vitro* motility assay. Data in **b** and **c** are mean values ± s.d. from three independent experiments.

pCa ≤ 5.6, all actin filaments were detached from myosin V, and thus sliding velocity could not be measured. Both the number and the velocity of sliding filaments could be restored to original levels by removing Ca^{2+} from the solution in the presence of 10 μM CaM (**Fig. 1**) but not in the absence of CaM (data not shown).

To determine the reason for the reduction in both the motility and the actin-binding affinity of myosin V, the number of CaM dissociated from myosin V in the presence of Ca^{2+} was estimated using single-molecule analysis. The dissociated CaM was substituted with Cy3-calmodulin (*CaM) and the number and intensity of fluorescent spots of *CaM were observed at single-molecule level (**Fig. 2a** and **Supplementary Methods** online). At pCa values of 6.0 and 5.8 (**Fig. 2b**), at least one CaM dissociated from each myosin V as the number of fluorescent spots (~0.19 spots μm^{-2}) of the substituted *CaM inside the chamber was almost equal to the calculated number of myosin V molecules initially applied to the chamber (binding of 0.025 nM myosin to the total contact area of 47×10^7 μm^2 in a chamber of 6 μl would give a value of ~0.19 molecules μm^{-2}). This number did not change after several washes with the Ca^{2+} solution followed by substitution with *CaM. In the absence of Ca^{2+} (pCa > 7.0) (**Fig. 2b**), only very few fluorescent spots could be detected (~10 spots) indicating that most of myosin V (~95%) was saturated with CaM before treatment with Ca^{2+}.

To quantify the effect of Ca^{2+} on the dissociation of CaM from myosin V, the dissociated CaM was substituted with *CaM and the population of single, double and triple substitutions of *CaM molecules (**Fig. 2c** and **Supplementary Methods** online) on the myosin V were estimated as a function of Ca^{2+} concentration (**Fig. 2d**). At pCa 6.2, ~50% of the myosin V molecules dissociated a single CaM molecule. At pCa 6.0, ~70% of myosin V dissociated a single CaM molecule, and ~30% of the myosin V dissociated two molecules. The dissociation of two CaM from one myosin V reached saturating levels at pCa 5.6. The triple bleaching steps were negligibly small (<5%) at all Ca^{2+} concentrations, whereas four or more bleaching steps were not observed. This suggests that each myosin V could lose a maximum of two CaM. To ensure that two was the maximum number, a sample was treated three times at pCa 5.2 after *CaM substitution and the number of spots having triple bleaching steps was still <5%.

Because it is well known that one CaM has four calcium-binding sites[3], the number of Ca^{2+} that binds to a CaM and triggers the dissociation of that CaM was estimated. The data for the dissociation of CaM from a myosin V in the presence of Ca^{2+} could be well fitted to the Hill equation giving a best fit value of 3.6 (**Fig. 2e**), suggesting that 3–4 Ca^{2+} are required to trigger the dissociation of one CaM.

Ca^{2+}-dependent dissociation rate of CaM

To determine the kinetic effect of Ca^{2+} on the regulation of myosin V motility, the dissociation rate of CaM from myosin V in the presence of Ca^{2+} was estimated by substituting the dissociated CaM with 100 nM *CaM. To answer whether the association rate of 100 nM *CaM to myosin V affected the estimation of dissociation rate or not, the association rate of 100 nM *CaM to myosin V had to be determined first (**Supplementary Methods** online). The time course of *CaM substitu-

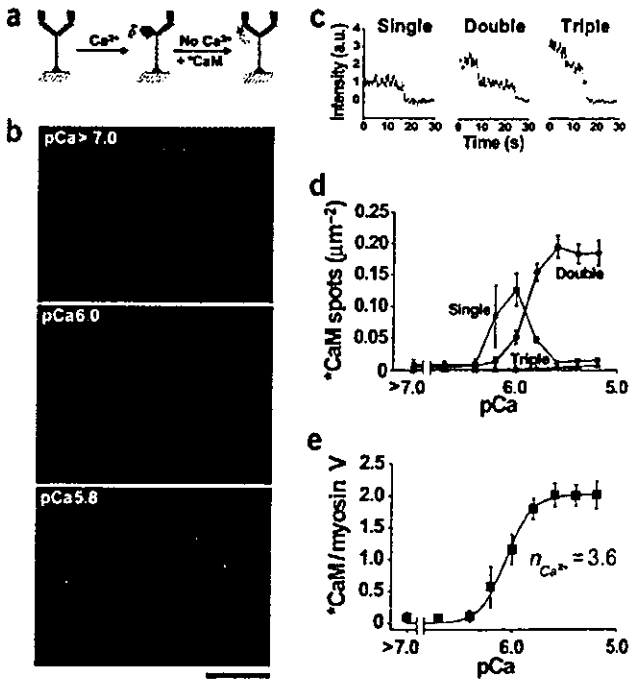

Figure 2 Effect of Ca^{2+} on the dissociation of CaM from myosin V. (**a**) Myosin V was treated with Ca^{2+} at various concentrations. The free Ca^{2+} was washed out and the dissociated CaM was substituted with *CaM. (**b**) Fluorescent spots of the substituted *CaM bound to individual myosin V on the glass surface were observed under TIRFM without Ca^{2+} treatment (pCa > 7.0) or after Ca^{2+} treatments at pCa 6.0 and 5.8. The density of myosin V was ~0.19 molecules μm^{-2} on the observation area (1,000 μm^2). Bar, 10 μm. (**c**) The bleaching steps of fluorescent intensity of single, double and triple *CaM molecules. (**d**) Number of *CaM substituted for CaM that dissociated from individual myosin V at different Ca^{2+} concentrations. (**e**) Dissociation of CaM (replaced with *CaM) from myosin V. Data were collected from D and fitted with the Hill equation[36] to determine the number of Ca^{2+} bound to CaM when CaM dissociates from myosin V. Data in **d** and **e** are mean values ± s.d. from three independent experiments.

© 2005 Nature Publishing Group http://www.nature.com/nsmb

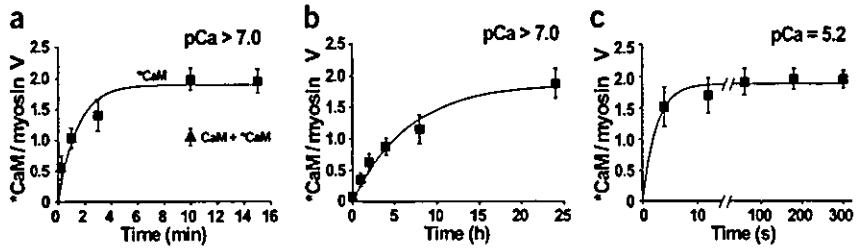

Figure 3 Ca^{2+}-dependent dissociation rate of CaM from myosin V (**Supplementary Methods** online). (**a**) The time course at 100 nM of *CaM substitution on myosin V that had lost a CaM in the absence of Ca^{2+}. Data were fitted with an exponential curve to obtain the association constant of *CaM to myosin V in the absence of Ca^{2+}. (**b**) The time course of *CaM exchange for CaM dissociated from myosin V in the absence of Ca^{2+}. Data were fitted with an exponential curve to obtain the dissociation constant of CaM from myosin V in the absence of Ca^{2+}. (**c**) The time course of CaM dissociated from myosin V at pCa 5.2, which was determined from the substitution of *CaM. Data were fitted with an exponential curve to obtain the dissociation constant of CaM from myosin V at pCa 5.2. Data are mean values ± s.d. from three independent experiments.

tion on myosin V was fitted to an exponential curve (**Fig. 3a**) to determine the pseudo first-order association rate constant ($[*CaM]k_{7.0+}$) at 100 nM *CaM in the absence of Ca^{2+}. To estimate the second-order association rate constant ($k_{7.0+}$), two similar experiments were done at 20 and 50 nM *CaM. The best-fit line on the graph of *CaM concentrations versus first-order association rate constants showed that $k_{7.0+}$ was $\sim 1 \times 10^5\ M^{-1}\ s^{-1}$ (data not shown). To confirm that labeling with Cy3 does not affect the association rate of *CaM, a 1:1 mixture of nonlabeled CaM and *CaM (100 nM each) was used in a similar experiment as described above. After a 10-min incubation, the number of re-bound *CaM was reduced to ~50% (**Fig. 3a**), indicating that Cy3 labeling had no substantial effect on the association rate of *CaM.

To measure the dissociation rate of CaM from myosin V in the absence of Ca^{2+}, myosin V bound to a glass surface was incubated with 100 nM *CaM for various periods of time up to 24 h (**Supplementary Methods** online). The data were fitted to an exponential curve (**Fig. 3b**) and the dissociation rate constant ($k_{7.0-}$) in the absence of Ca^{2+} was $\sim -0.4 \times 10^{-5}\ s^{-1}$. The dissociation constant (K_d) of CaM from myosin V in the absence of Ca^{2+} was calculated as $k_{7.0-} / k_{7.0+}$, giving a value of ~0.4 nM. To determine the dissociation rate of CaM in the presence of Ca^{2+} (**Supplementary Methods** online), the time course of CaM dissociated from myosin V at pCa 5.2 was fitted to an exponential curve (**Fig. 3c**). The dissociation rate constant ($k_{5.2-}$) at pCa 5.2 was $\sim -0.4\ s^{-1}$, which is 10^5 times faster than that in the absence of Ca^{2+}.

Regulation of myosin V by caged Ca^{2+}

The conventional *in vitro* motility assay does not show the transient effect of Ca^{2+} on myosin V that normally occurs in cells. To overcome this limitation, the sliding of the filaments was regulated by incorporating an *in vitro* motility assay with caged Ca^{2+} that can generate Ca transients using a UV flash (**Supplementary Methods** online). The duration of the UV flash is 4 s. Before the UV flash, actin filaments moved smoothly on the glass surface (**Fig. 4a(i)**). At the end of the UV flash, most of actin filaments had detached (**Fig. 4a(ii)**), and 40 s after the completion of the UV flash most of them had reattached (**Fig. 4a(iii)**) (**Supplementary Video 1** online).

The time course of the Ca^{2+} concentration was measured using Rhod-2 (ref. 22), a Ca^{2+}-sensitive fluorophore (**Fig. 4b**). Quantification of the number of sliding actin filaments and velocity at which these filaments were moving under various concentrations of CaM show that, before the UV flash, there were ~0.15 actin filaments μm^{-2} sliding at ~400 nm s^{-1} (**Fig. 4c,d**). Within a second after starting the UV flash, actin filaments became detached in the illumination area (**Fig. 4c**). In the absence of free CaM, the number of sliding actin filaments did not increase, even after several minutes (data not shown). In contrast, in the sample containing free CaM, actin filaments were able to gradually reattach and the rate of reattachment was dependent on the free CaM concentration. During the UV flash and before detachment of the actin filaments, the velocity slowed to ~230 nm s^{-1}. When the UV illumination was completed, the velocity was gradually increased and the acceleration was dependent on the free CaM concentration (**Fig. 4d**). The velocity of sliding in the samples could not be measured without adding free CaM, as otherwise the actin filaments did not attach. The number and velocity of sliding actin filaments remained unchanged using UV flash in the absence of caged Ca^{2+} (data not shown). In conclusion, using photolysis of caged Ca^{2+}, we observed the transient regulation of the number of actin filaments and their sliding velocity in the *in vitro* motility assay of myosin V. The movement commenced with detachment and then slowed within a few seconds. Finally, the filaments reattachment and movement recommenced in the presence of free CaM.

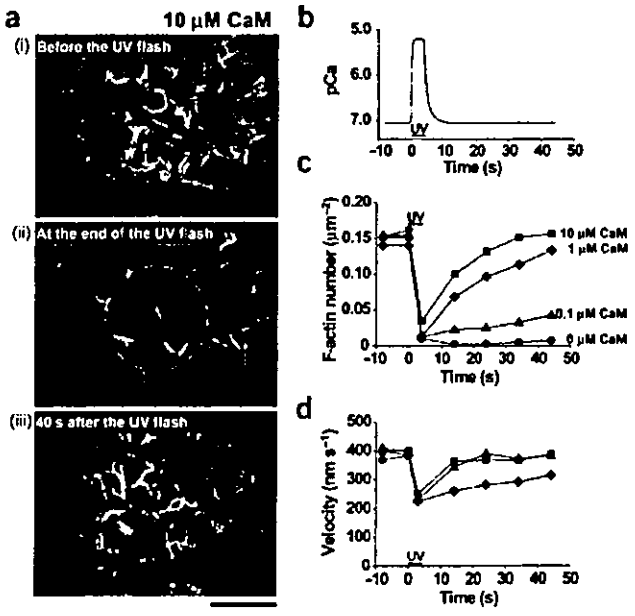

Figure 4 Reversible regulation of myosin V function with transient Ca^{2+} generated by UV photolysis of caged Ca^{2+}. The *in vitro* motility assay was carried out in the presence of transient Ca^{2+} concentrations, which were generated locally by UV photolysis of caged Ca^{2+} within a time frame of 4 s. (**a**) Experiments in the presence of 10 μM CaM at the moment just before (i), at the end of the flash (ii), and 40 s after the 4-s UV photolysis of caged Ca^{2+} (iii). Bar, 10 μm; circle, UV illumination area (**Supplementary Video 1** online). (**b**) The transient Ca^{2+} concentration generated by a 4-s flash of UV photolysis of caged Ca^{2+} was measured using Rhod-2 as the signal. (**c,d**) Effects of the transient Ca^{2+} concentration on the number (**c**) and velocity (**d**) of sliding actin filaments (F-actin) at various CaM concentrations. Data in **c** and **d** are mean values from three independent experiments.

© 2005 Nature Publishing Group http://www.nature.com/nsmb

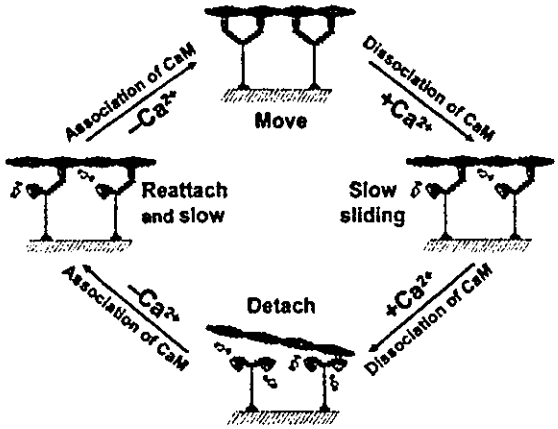

Figure 5 Model for the reversible regulation of myosin V motor functions by Ca^{2+} in the presence of free CaM. In the absence of Ca^{2+} (pCa > 7.0) (move) the actin filaments slide on myosin V with both heads intact. When the Ca^{2+} concentration increased to pCa ≅ 6.0 (slow sliding), one CaM was lost from one of the myosin heads. The single intact head was still able to move the actin filaments by multiple molecules of myosin V but at a velocity ~60% slower than that of native myosin V. When the Ca^{2+} concentration increased to pCa ≤ 5.6 (detach), myosin V lost both CaM from each of the two heads and the actin filaments became detached from myosin V. When the Ca^{2+} concentration returned to the normal low level, free CaM quickly bound to the vacant IQ motif and myosin V quickly recovered to the single-headed active stage (reattach and slow) and the stage of two heads regained their normal function (move). The structure of the motor domain folding back to the neck domain was adapted from a reported structure[27].

© 2005 Nature Publishing Group http://www.nature.com/nsmb

DISCUSSION

In the *in vitro* motility assay, actin filaments exhibited a slow sliding velocity at pCa 6.0 and detached at pCa ≤ 5.6. The sliding velocity and number of attached actin filaments could be restored after washing out Ca^{2+} in the presence of free CaM (Fig. 1a–c), but could not be restored after washing out Ca^{2+} in the absence of free CaM. This indicates that the slowing of movement and detachment of actin filaments are due to the dissociation of CaM.

Regulation of myosin V by single CaM

In previous studies, the number of CaM that dissociated from myosin V at certain Ca^{2+} concentrations was estimated by measuring the change in stoichiometry of CaM per heavy chain using a gel scanning method[20,23]. However, the method does not show the distribution of the number of CaM molecules dissociated from an individual myosin molecule. The exact number of CaM that dissociated also could not be estimated owing to the limitations in resolution using this gel scanning method, because the dissociation of a single CaM molecule from a total of 12 bound[24] to myosin V needed to be observed. These limitations were overcome by using single-molecule imaging techniques to evaluate the exact number of single CaM molecules dissociated from individual molecules of a native myosin V at various pCa values. The results showed that the process of CaM dissociation at gradient Ca^{2+} concentrations includes several distinct dissociation events. In a 3-min incubation at pCa 6.0, at least one or two CaM molecules dissociated from each myosin, and at pCa 5.6, two CaM dissociated from every myosin; this is thought to be the maximum number (Fig. 2c). This suggests that one CaM originally dissociated from one heavy chain at a single specific IQ motif, because the myosin V is a homodimer[16]. If this were not the case, the number would be >2. We observed the dissociation of two CaM when myosin V was treated at physiological concentrations of Ca^{2+} (pCa > 5.0)[25], as well as at very high concentrations of Ca^{2+} (pCa 4.5) for 10 s. However, ~15% of the myosin V molecules dissociated three CaM molecules or more when the myosin V was treated at pCa 4.5 for 5 min (data not shown). This agrees with the data from a previous study[26] in which ~2.1 CaM dissociated when CaM was exchanged with *CaM by treatment of myosin V with a solution containing 1 mM EGTA and 1.01 mM $CaCl_2$ (pCa ≅ 4.6) for 5 min. Using the same method, another group of researchers[13] obtained a myosin V mixture containing ~76% of the labeled CaM exchanged at the IQ motif at the end of neck domain connecting to the head of myosin V. Their findings also suggested that a single CaM molecule dissociated from a specific site on the myosin V heavy chain.

The good correlation between the number of sliding actin filaments and the dissociation of single CaM molecules from myosin V suggests that actin-binding affinity is regulated by the dissociation of single CaM molecules. The dissociation of CaM from heavy chains results in a conformational change to the head and neck region of the myosin V molecule[27]. The head-neck domain of myosin V is extended in the absence of Ca^{2+}, whereas at high Ca^{2+} concentrations, the head domain folds back onto the neck domain; this may reduce the actin-binding affinity of the myosin head. The reduction of actin-binding affinity of the myosin head at high Ca^{2+} concentration was also supported by the biochemical results of the actin-activated ATPase activity measured under similar conditions to our motility assay (100 mM KCl; 25 °C). At high Ca^{2+} concentrations, the $K_{m,actin}$ of single-headed myosin V (19.9 μM) is about two-fold higher compared with that in the absence of Ca^{2+} (9.2 μM)[27]. The increase of $K_{m,actin}$ suggests that the actin-binding affinity of the myosin head was reduced at high Ca^{2+} concentrations. This may disrupt the overlap between the two heads of a myosin V, which would reduce the processivity of double-headed myosin V, causing the detachment of sliding actin filament. The high Ca^{2+} concentrations (>1 μM) reduce the actin-binding affinity of the myosin V head through the dissociation of single CaM molecules by binding Ca^{2+} and folding back of the head domain onto the neck. In contrast to glass binding myosin V, in solution the intact myosin V strongly binds to actin filament in the presence of Ca^{2+} (ref. 28); thus the ATPase activity remains high.

We characterized the kinetics of the Ca^{2+}-dependent dissociation of CaM from myosin V at a single-molecule level. In the absence of Ca^{2+}, CaM binds very rapidly and with a high affinity to myosin V, maintaining a stable association of CaM with myosin V for a functional motor at normal low cellular Ca^{2+} concentrations. In the presence of Ca^{2+}, the rapid dissociation of CaM (within seconds) allows myosin V to be regulated by transient Ca^{2+} bursts in cells.

Transient regulation of myosin V

Myosin V is abundantly expressed in nerve cells[15]. It has also been reported that the tips of filopodia (the finger-like projections on the tips of developing nerve cells) generate tiny bursts of Ca^{2+} that travel back to the growth cone to stimulate movement in the correct direction[29]. We simulated the cellular Ca^{2+} bursts by using caged Ca^{2+} coupled with a UV flash system to generate Ca^{2+} transients locally within a time range of a few seconds in an *in vitro* motility assay. We observed a quick response of myosin V motor functions as demonstrated by the detachment of filaments and a reduction in velocity of actin filament sliding during the UV flash. Compared with samples containing 10 or 1 μM CaM, the slower recovery in the case of 0.1 μM CaM and the fact that no recovery occurred in the absence of free CaM support our conclusion that CaM dissociation is involved in the regulation of actin-binding affinity and motility of myosin V. Although the association rate of CaM is very quick in the absence of Ca^{2+} (<1 s at 10 μM CaM) the reattachment of the actin filaments was slower, probably because of the low concentration of actin filaments in the medium.

Model for the regulation of myosin V

We propose a model for the transient regulation of various myosin V functions by Ca^{2+} (Fig. 5). In the absence of Ca^{2+}, the native myosin V has a full complement of bound CaM and moves the actin filaments with both heads. When the Ca^{2+} concentration increased to pCa ≅ 6.0, one of the two heads of myosin V lost one CaM and myosin was in the single-headed active stage. At this stage, the actin-binding affinity was partially reduced and the velocity was slow. Increasing the Ca^{2+} concentration further (pCa 5.6), caused the other head of myosin V to also lose one CaM. Myosin V then moved to the double-headed inactive stage, causing the actin filaments to detach. When Ca^{2+} was chelated, the free CaM quickly rebound to one of the heads that had lost a CaM and myosin V once again was in the single-headed active stage. Finally, the second CaM associated with myosin V and both heads bound a CaM, in what is known as the double-headed active stage of myosin V. In conclusion, the binding of 3–4 Ca^{2+} to one CaM (Fig. 2e) triggers the dissociation of a single CaM molecule from each myosin head, causing a reduction in actin-binding affinity and in the sliding velocity of myosin V. This model of the regulation of myosin V by Ca^{2+} involving various intermediate stages could be useful in understanding how CaM-binding motor proteins bind, move, detach, rebind and move again on actin filament tracks in cells.

METHODS

Chemicals and proteins. Bovine brain CaM was obtained from Sigma. Alexa-647-phalloidin, *o*-nitrophenyl EGTA tetrapotassium salt[30] and Ca^{2+}-sensitive bright Rhod-2 tripotassium salt were obtained from Molecular Probes. Myosin V was purified from chick brains[24]. G-actin was purified from chicken breast muscle[31]. Actin filaments were prepared by polymerization of G-actin in high-salt solution and labeled with Alexa-647-phalloidin. *CaM was prepared as described[26] except that the buffer for labeling was adjusted to pH 7.2 for specific labeling at the N terminus. The obtained *CaM has a Cy3/CaM mole ratio of 1.04:1. *CaM bound to a glass surface in 20 mM HEPES, pH 7.2, was observed as single spots for ~20 s and photobleached in one step, proving that purified *CaM were indeed single molecules.

Buffers and solutions. Buffer A contained 25 mM K-acetate, 100 mM KCl, 4 mM $MgCl_2$, 10 mg ml^{-1} BSA, 1 mM EGTA and 20 mM HEPES, pH 7.2 (pCa > 7.0). EGTA-Ca^{2+} solutions with different free Ca^{2+} concentrations were adjusted by mixing various ratios of buffer A with solution B (buffer A supplemented with 1.05 mM $CaCl_2$). The free Ca^{2+} concentration in the mixture[32] was calculated based on the K_d of EGTA-Ca^{2+}. An oxygen scavenger system[33] was added to all buffers for all imaging experiments.

Single-molecule microscopy. The sealed chambers of all assays were observed under total internal reflection fluorescence microscopy (TIRFM)[33,34]. *CaM and Rhod-2 were excited by a Nd:YAG laser (TIM-6222, Transverse) at 532 nm. Alexa-647-labeled actin filaments were excited by a diode laser (F44-30M, Coherent) at 635 nm. The image was recorded on a DVD recorder (DVR-7000; Pioneer). UV flashes for caged Ca^{2+} activation[35] were created by a 100-W high-pressure mercury lamp, passed through a band-pass filter of 340–370 nm, controlled with a shutter, passed through the objective lens and at last focused into the chamber solution.

Slide quartz glasses, cover glasses and spacers (25-μm thick) were sonicated with 0.1 M KOH and then with 5 M HCl and rinsed with distilled water before use to reduce the background interference for single-molecule imaging and to reduce the effect on the motility activity of myosin V in an *in vitro* motility assay. The chamber was assembled using a slide quartz glass, a cover glass and two spacers. The chamber volume was ~6 μl.

***In vitro* motility assay of myosin V.** The *in vitro* motility assays of myosin V were carried out in the absence and presence of Ca^{2+}. In the presence of Ca^{2+}, the Ca^{2+} concentration was changed in a stepwise or transient manner, depending on the purpose of the experiment (**Supplementary Methods** online).

Substitution of CaM with Cy3-CaM. A flow glass chamber was rinsed with BSA in 10 μl buffer A, and exchanged with 6 μl of 0.025 nM myosin V in buffer A (~0.19 molecules μm^{-2}) for 2 min to allow the myosin to bind to the glass surface. The slide was then treated with 10 μl of the Ca^{2+} solution for 3 min. The free Ca^{2+} was washed out and the dissociated CaM was substituted with 20 μl of 100 nM *CaM in buffer A for 10 min (10 min was sufficient for most of the dissociated CaM to be substituted (**Fig. 3a**) and was also enough time for restoration of myosin V motility back to almost 'normal' levels; data not shown). Finally, the free *CaM was washed by incubation with 20 μl buffer A for 3 min. *CaM bound on myosin V was observed under TIRFM after exchange of the buffer with buffer A supplemented with an oxygen scavenger system.

The majority of the dissociated CaM was substituted with *CaM within 5 min (**Fig. 3a**) and observations could be made for at least 1 h under TIRFM without affecting the number or the intensity of the substituted *CaM fluorescent spots. This indicates that in the presence of 100 nM *CaM and in the absence of Ca^{2+}, the dissociation rate of CaM from myosin V is negligibly slow compared with the association rate (at least ten times slower). The number of substituted *CaM fluorescent spots indicates the number of CaM-dissociated myosin V molecules because almost no spots (0.6% compared with sample in the presence of myosin V) were observed in the absence of myosin V.

For determination of the association and dissociation rate of CaM from myosin V, see **Supplementary Methods** online.

All mentioned assays were done at 25 °C.

Note: Supplementary information is available on the Nature Structural & Molecular Biology website.

ACKNOWLEDGMENTS

We thank N. Sasaki and S. Uemura for giving important suggestions and helping in purification of myosin V, and T. Ando and J. M. West for critical reading of the manuscript. The research was supported by Grants-in-Aid for Scientific Research in Priority Areas from the Japan Ministry of Education, Culture, Sports, Science and Technology (H.H.). H.A.N. was the recipient of a postdoctoral scholarship from the Japan Society for the Promotion of Science.

COMPETING INTERESTS STATEMENT

The authors declare that they have no competing financial interests.

Received 14 October; accepted 16 December 2004
Published online at http://www.nature.com/nsmb/

1. Ikura, M. Calcium binding and conformational response in EF-hand proteins. *Trends Biochem. Sci.* **21**, 14–17 (1996).
2. Chin, D. & Means, A.R. Calmodulin: a prototypical calcium sensor. *Trends Cell Biol.* **10**, 322–328 (2000).
3. Prekeris, R. & Terrian, D.M. Brain myosin V is a synaptic vesicle–associated motor protein: evidence for a Ca^{2+}-dependent interaction with the synaptobrevin–synaptophysin complex. *J. Cell Biol.* **137**, 1589–1601 (1997).
4. Evans, L.L., Lee, A.J., Bridgman, P.C. & Mooseker, M.S. Vesicle-associated brain myosin V can be activated to catalyze actin-based transport. *J. Cell Sci.* **111**, 2055–2066 (1998).
5. Tabb, J.S., Molyneaux, B.J., Cohen, D.L., Kuznetsov, S.A. & Langford, G.M. Transport of ER vesicles on actin filaments in neurons by myosin V. *J. Cell Sci.* **111**, 3221–3234 (1998).
6. Provance, D.W. Jr., Wei, M., Ipe, V. & Mercer, J.A. Cultured melanocytes from dilute mutant mice exhibit dendritic morphology and altered melanosome distribution. *Proc. Natl. Acad. Sci. USA* **93**, 14554–14558 (1996).
7. Wu, X., Bowers, B., Wei, Q., Kocher, B. & Hammer, J.A. 3rd. Myosin V associates with melanosomes in mouse melanocytes: evidence that myosin V is an organelle motor. *J. Cell Sci.* **110**, 847–859 (1997).
8. Karcher, R.L. *et al.* Cell cycle regulation of myosin V by calcium/calmodulin-dependent protein kinase II. *Science* **293**, 1317–1320 (2001).
9. Hill, K.L., Catlett, N.L. & Weisman, L.S. Actin and myosin function in directed vacuole movement during cell division in *Saccharomyces cerevisiae*. *J. Cell Biol.* **135**, 1535–1549 (1996).
10. Catlett, N.L. & Weisman, L.S. The terminal tail region of a yeast myosin V mediates its attachment to vacuole membranes and sites of polarized growth. *Proc. Natl. Acad. Sci. USA* **95**, 14799–14804 (1998).
11. Mehta, A.D. *et al.* Myosin V is a processive actin-based motor. *Nature* **400**, 590–593 (1999).
12. Uemura, S., Higuchi, H., Olivares, A.O., De La Cruz E.M. & Ishiwata, S. Mechanochemical coupling of 12- and 24-nm substeps in a single myosin V motor. *Nat. Struct Mol. Biol.* **11**, 877–883 (2004).
13. Yildiz, A. *et al.* Myosin V walks hand-over-hand: single fluorophore imaging with 1.5-nm localization. *Science* **300**, 2061–2065 (2003).
14. Espindola, F.S. *et al.* Biochemical and immunological characterization of p190–calmodulin complex from vertebrate brain: a novel calmodulin binding myosin. *J. Cell Biol.* **118**, 359–368 (1992).

© 2005 Nature Publishing Group http://www.nature.com/nsmb

15. Espreafico, E.M. *et al.* Primary structure and cellular localization of chicken brain myosin V (p190), an unconventional myosin with calmodulin light chains. *J. Cell Biol.* **119**, 1541–1557 (1992).
16. Cheney, R.E. *et al.* Brain myosin V is a two-headed unconventional myosin with motor activity. *Cell* **75**, 13–23 (1993).
17. Cameron, L.C. *et al.* Calcium-induced quenching of intrinsic fluorescence in brain myosin V is linked to dissociation of calmodulin light chains. *Arch. Biochem. Biophys.* **355**, 35–42 (1998).
18. Nascimento, A.A., Cheney, R.E., Tauhata, S.B., Larson, R.E. & Mooseker, M.S. Enzymatic characterization and functional domain mapping of brain myosin V. *J. Biol. Chem.* **271**, 17561–17569 (1996).
19. Trybus, K.M., Krementsova, E. & Freyzon, Y. Kinetic characterization of a monomeric unconventional myosin V construct. *J. Biol. Chem.* **274**, 27448–27456 (1999).
20. Homma, K., Saito, J., Ikebe, R. & Ikebe, M. Ca^{2+}-dependent regulation of the motor activity of myosin V. *J. Biol. Chem.* **275**, 34766–34771 (2000).
21. Martin, S.R. & Bayley, P.M. Regulatory implications of a novel mode of interaction of calmodulin with a double IQ motif target sequence from murine dilute myosin V. *Protein Sci.* **11**, 2909–2923 (2002).
22. Nguyen, V.T., Higuchi, H. & Kamio, Y. Controlling pore assembly of staphylococcal γ-haemolysin by low temperature and by disulphide bond formation in double-cysteine LukF mutants. *Mol. Microbiol.* **45**, 1485–1498 (2002).
23. Krementsov, D.N., Krementsova, E.B. & Trybus, K.M. Myosin V: regulation by calcium, calmodulin, and the tail domain. *J. Cell Biol.* **164**, 877–886 (2004).
24. Cheney, R.E. Purification and assay of myosin V. *Methods Enzymol.* **298**, 3–18 (1998).
25. Poenie, M., Alderton, J., Tsien, R.Y. & Steinhardt, R.A. Changes of free calcium levels with stages of the cell division cycle. *Nature* **315**, 147–149 (1985).
26. Sakamoto, T., Amitani, I. Yokota, E. & Ando, T. Direct observation of processive movement by individual myosin V molecules. *Biochem. Biophys. Res. Commun.* **272**, 586–590 (2000).
27. Li, X.D., Mabuchi, K., Ikebe, R. & Ikebe, M. Ca^{2+}-induced activation of ATPase activity of myosin Va is accompanied with a large conformational change. *Biochem. Biophys. Res. Commun.* **12**, 538–545 (2004).
28. Tauhata, S.B., dos Santos, D.V., Taylor, E.W., Mooseker, M.S. & Larson, R.E. High affinity binding of brain myosin Va to F-actin induced by calcium in the presence of ATP. *J. Biol. Chem.* **276**, 39812–39818 (2001).
29. Gomez, T.M., Robles E., Poo M. & Spitzer N.C. Filopodial calcium transients promote substrate-dependent growth cone turning. *Science* **291**, 1983–1987 (2001).
30. Ellis-Davies, G.C. & Kaplan, J.H. Nitrophenyl-EGTA, a photolabile chelator that selectively binds Ca^{2+} with high affinity and releases it rapidly upon photolysis. *Proc. Natl. Acad. Sci. USA* **91**, 187–191 (1994).
31. Spudich, J.A. & Watt, S. The regulation of rabbit skeletal muscle contraction. I. Biochemical studies of the interaction of the tropomyosin troponin complex with actin and the proteolytic fragments of myosin. *J. Biol. Chem.* **246**, 4866–4871 (1971).
32. Horiuti, K. *et al.* Mechanism of action of 2,3-butanedione 2-monoxime on contraction of frog skeletal muscle fibres. *J. Muscle. Res. Cell Motil.* **9**, 156–164 (1988).
33. Nguyen, V.T., Kamio, Y. & Higuchi, H. Single molecule imaging of cooperative assembly of γ-hemolysin on erythrocyte membranes. *EMBO J.* **22**, 4968–4979 (2003).
34. Funatsu, T., Harada, Y., Tokunaga, M., Saito, K. & Yanagida, T. Imaging of single fluorescent molecules and individual ATP turnovers by single myosin molecules in aqueous solution. *Nature* **374**, 555–559 (1995).
35. Dantzig, J.A., Higuchi, H. & Goldman, Y.E. Studies of molecular motors using caged compounds. *Methods Enzymol.* **291**, 307–348 (1998).
36. West, J.M., Higuchi, H., Ishijima, A. & Yanagida, T. Modification of the bi-directional sliding movement of actin filaments along native thick filaments isolated from a clam. *J. Muscle Res. Cell Motil.* **17**, 637–646 (1996).

© 2005 Nature Publishing Group http://www.nature.com/nsmb

SUPPLEMENTARY METHODS

In vitro motility assay of myosin V

The assay was performed at various Ca^{2+} concentrations. After flushing the chamber with 10 μl buffer A, the chamber was filled with 6 μl of 10 nM myosin V for a period of 2 min. Finally, the solution in the chamber was exchanged with buffer containing free Ca^{2+} supplemented with 150 nM Alexa–647 labeled actin filaments, 1 mM ATP and an oxygen scavenger system. The number of sliding labeled actin filaments was counted and averaged from ten observed areas. The velocity was measured and averaged from ten actin filaments.

For restoration of the myosin V motility, myosin V was treated with free Ca^{2+} at pCa 5.2 for 3 min and then its motile activity restored by washing out free Ca^{2+}, followed by incubation with 10 μM CaM for 5 min. The excessive CaM was washed out before performing *in vitro* motility assay. The percentage of moving actin filaments was estimated and averaged from five observed areas.

For the regulation of actin filaments sliding on myosin V using transient Ca^{2+} concentrations[35], the final solution contained Ca^{2+} at pCa 5.0 with the addition of 1 mM NP–EGTA. During the motility assay, an area of the glass ~17 μm in diameter containing myosin V was locally illuminated with UV for a period of 4 s.

To measure the local transient Ca^{2+} concentration inside the chamber, 10 nM Rhod–2, a Ca^{2+} sensitive fluorophore[22], was added to the solution in the chamber and the fluorescent intensity monitored. The standard curve for the relationship between the Rhod–2 fluorescent intensity and Ca^{2+} concentration was prepared using solutions, with pre–determined free Ca^{2+} concentrations.

Estimation the number of dissociated CaM

Myosin V bound to a glass surface (~0.19 molecules μm^{-2}) was treated for 3 min with 10 μl of solution of Ca^{2+} ranging from less than pCa 7.0 to pCa 5.2. The dissociated CaM from myosin V was substituted with 20 μl of 100 nM *CaM in buffer A for 10 min. The free *CaM was washed out with 20 μl buffer A for 3 min. *CaM bound on myosin V was observed under TIRFM. The number of spots is equal to the number of myosin V molecules from which one CaM molecule or more was dissociated. To avoid the overlap of more than one myosin V molecules at the same position, the experiment was performed at low concentration of myosin V.

The intensity of light emitted from a single *CaM is relatively stable. However the emitted light is photobleached within tens of seconds of illumination. Thus the number of *CaM on each spot was estimated by counting the bleaching step of the intensity. Each step corresponds to the one *CaM molecule.

Association rate constant of single CaM molecules to myosin V in the absence of Ca^{2+}

Myosin V bound to a glass surface (~0.19 molecules μm^{-2}) was treated with 10 μl of solution (pCa 5.2) for 3 min. The dissociated CaM from myosin V was substituted with 20 μl of 100 nM *CaM in buffer A for various periods of time up to 15 min. The substitution was stopped by washing out the free *CaM with 20 μl buffer A for 3 min. *CaM bound on myosin V was observed under TIRFM. The following reaction occurs:

$$*CaM + IQ \underset{k_{7.0-}}{\overset{k_{7.0+}}{\rightleftharpoons}} *CaM\text{–}IQ$$

IQ is the IQ motif of myosin V on which the CaM was dissociated from. $k_{7.0+}$ and $k_{7.0-}$ are the association and dissociation rate constant in the absence of Ca^{2+} (pCa > 7.0), respectively.

At 100 nM *CaM and in the absence of Ca^{2+}, the dissociation rate of *CaM from myosin V is negligibly slow compared to the association rate ($k_{7.0+}$[*CaM] >> $k_{7.0-}$). The $k_{7.0+}$ could be determined by fitting the experimental data into an exponential curve:

$$[*CaM\text{–}IQ] / [IQ_o] = 1 - e^{-[*CaM]\,k7.0+t}$$

Where $[IQ_o]$ is the total number of IQ available for the substitution of *CaM at time 0, [*CaM–IQ] is the number of substituted *CaM, t is the time for taken for the substitution.

Dissociation rate constant of CaM from myosin V in the absence of Ca^{2+}

Myosin V bound on a glass surface (~0.19 molecules μm^{-2}) was incubated with 100 nM *CaM in buffer A (pCa > 7.0) for various times up to 24 h in order to complete the substitution with CaM. The reaction was stopped by washing free *CaM with 20 μl buffer A for 3 min. *CaM bound to myosin V was observed under TIRFM. As [*CaM] >> [CaM] (4000 times), the association rate of CaM to IQ is negligibly small compared to that of *CaM to IQ. At 100 nM *CaM and in the absence of Ca^{2+}, the dissociation rate of *CaM from myosin V is negligibly slow compared to the association rate. This can be described by the following reactions:

$$CaM\text{–}IQ \xrightarrow{k_{7.0-}} IQ + CaM \qquad (1)$$

$$*CaM + IQ \xrightarrow{k_{7.0+}} *CaM\text{–}IQ \qquad (2)$$

As reaction (1) is the rate limiting step for the two reactions, the $k_{7.0-}$ can be determined by fitting the experimental data of exchanged *CaM number to the exponential curve:

$$[*CaM\text{–}IQ] / [CaM\text{–}IQ_o] = 1 - e^{-k7.0-t}$$

Where, [*CaM–IQ] is the number of exchanged *CaM, [CaM–IQ_o] is the total number of CaM–IQ that could participate in the reaction at time 0, and t is the incubation time for exchanging.

Dissociation rate constant of CaM from myosin V at pCa 5.2.

Myosin V bound on a glass surface (~0.19 molecules μm^{-2}) was treated at pCa 5.2 at various times for up to 300 s at a time, in the presence of 100 nM *CaM. The free Ca^{2+} was washed out with 20 μl of 100 nM *CaM in buffer A and the incubation continued for 10 more minutes. *CaM bound myosin V was observed under TIRFM.

During treatment of myosin V with *CaM at pCa 5.2, as [*CaM] >> [CaM], the association rate of CaM and IQ is negligibly small, compared to the rate of *CaM to IQ. This can be described by the following reactions:

$$CaM\text{–}IQ \xrightarrow{k_{5.2-}} CaM + IQ \qquad (1)$$

$$*CaM + IQ \underset{k_{5.2-}}{\overset{k_{5.2+}}{\rightleftharpoons}} *CaM\text{–}IQ \qquad (2)$$

$k_{5.2+}$ and $k_{5.2-}$ are the association and dissociation rate constants at pCa 5.2, respectively. In the next step of the experiment, free Ca^{2+} was removed to stop the reaction (2) in the presence of 100 nM *CaM. Reaction (2) therefore becomes:

$$*CaM + IQ \xrightarrow{k_{7.0+}} *CaM\text{–}IQ \qquad (3)$$

The CaM dissociated IQ number in (1) was indicated by total number of *CaM–IQ in (2) and (3) which was observed under TIRFM. The $k_{5.2-}$ in reaction (1) could be determined by fitting the experimental data of observed *CaM–IQ number to the exponential curve:

$$[*CaM\text{–}IQ] / [CaM\text{–}IQ_o] = 1 - e^{-k5.2-t}$$

Where, [*CaM–IQ] is the number of observed *CaM–IQ, [CaM–IQ_o] is the total number of CaM–IQ that could release CaM at time 0 after incubation at pCa 5.2, and t is the treatment time at pCa 5.2.

The PDF file of Supplementary Methods was prepared by HoaAnh Nguyen

Supplementary Video 1

The reversible attachment and movement of actin filaments by myosin V.

An *in vitro* motility was performed in the presence of 10 μM CaM and transient Ca^{2+} concentrations, which was generated locally by UV photolysis of caged Ca^{2+} within a time frame of 4 s. The number indicates the time in seconds and tens of milliseconds. The time period of the UV flash was indicated by "UV". Bar 10 μm. This movie is a supplement for Figure 4a.

Before the UV flash

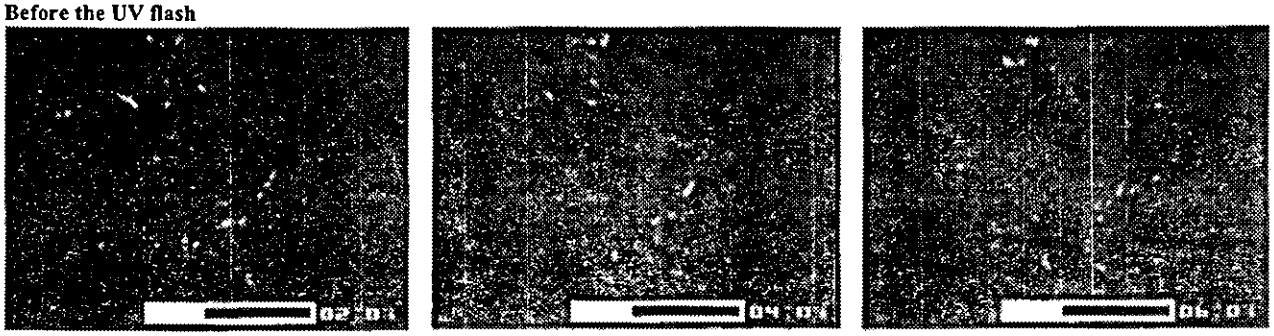

During the UV flash

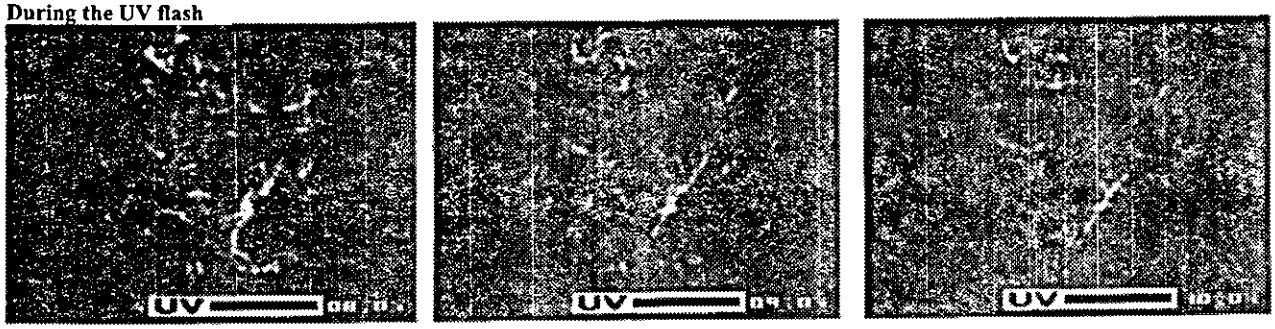

Several seconds after the UV flash

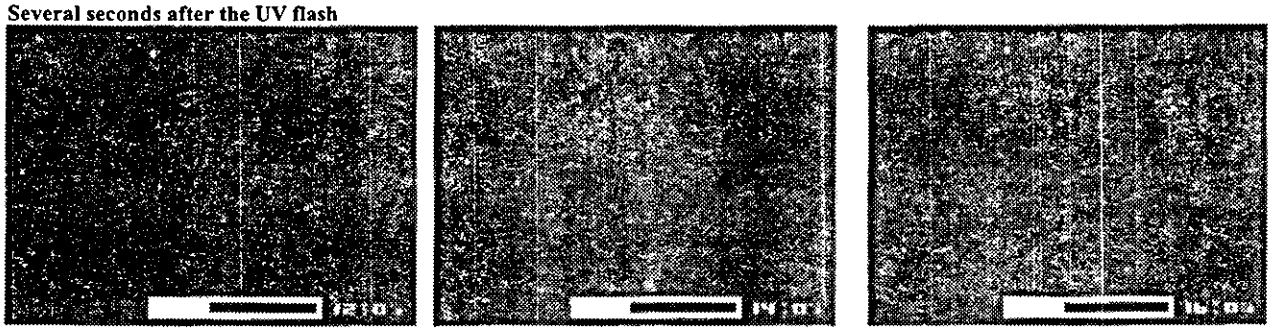

Tens-second after the UV flash

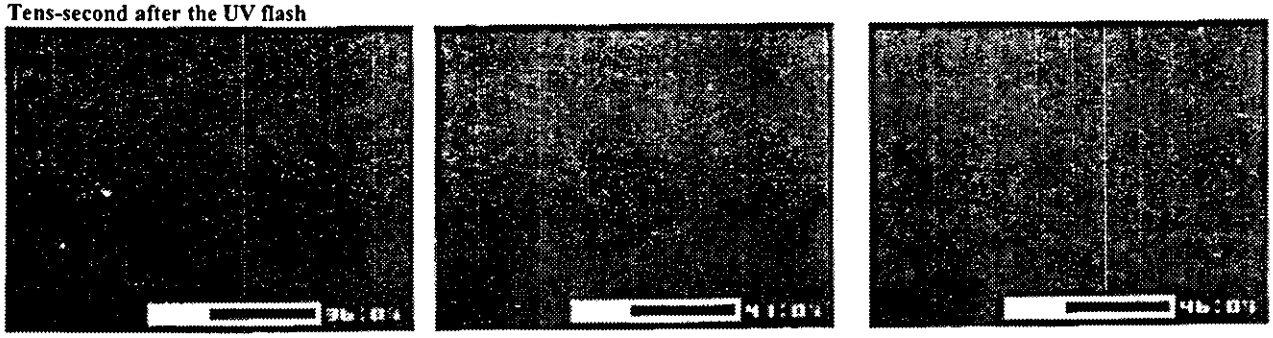

Am J Physiol Cell Physiol 287: C603–C611, 2004.
First published May 26, 2004; 10.1152/ajpcell.00347.2003.

Regional rheological differences in locomoting neutrophils

M. Yanai,[1,2] J. P. Butler,[1,4] T. Suzuki,[1,2] H. Sasaki,[1] and H. Higuchi[2,3]

[1]*Department of Geriatric and Respiratory Medicine, Tohoku University School of Medicine, Sendai 980-8574;* [2]*Center for Interdisciplinary Research, Tohoku Univ., Sendai 980;* [3]*Department of Metallurgy, Graduate School of Engineering, Tohoku University, Sendai 980, Japan; and* [4]*Harvard School of Public Health and Harvard Medical School, Boston, Massachusetts 02115*

Submitted 12 August 2003; accepted in final form 26 March 2004

Yanai, M., J. P. Butler, T. Suzuki, H. Sasaki, and H. Higuchi. Regional rheological differences in locomoting neutrophils. *Am J Physiol Cell Physiol* 287: C603–C611, 2004. First published May 26, 2004; 10.1152/ajpcell.00347.2003.—Intracellular rheology is a useful probe of the mechanisms underlying spontaneous or chemotactic locomotion and transcellular migration of leukocytes. We characterized regional rheological differences between the leading, body, and trailing regions of isolated, adherent, and spontaneously locomoting human neutrophils. We optically trapped intracellular granules and measured their displacement for 500 ms after a 100-nm step change in the trap position. Results were analyzed in terms of simple viscoelasticity and with the use of structural damping (stress relaxation follows a power law in time). Structural damping fit the data better than did viscoelasticity. Regional viscoelastic stiffness and viscosity or structural damping storage and loss moduli were all significantly lower in leading regions than in pooled body and/or trailing regions (the latter were not significantly different). Structural damping showed similar levels of elastic and dissipative stresses in body and/or trailing regions; leading regions were significantly more fluidlike (increased power law exponent). Cytoskeletal disruption with cytochalasin D or nocodazole made body and/or trailing regions ~50% less elastic and less viscous. Cytochalasin D completely suppressed pseudopodial formation and locomotion; nocodazole had no effect on leading regions. Neither drug changed the dissipation-storage energy ratio. These results differ from those of studies of neutrophils and other cell types probed at the cell membrane via β_2-integrin receptors, which suggests a distinct role for the cell cortex or focal adhesion complexes. We conclude that *1*) structural damping well describes intracellular rheology, and *2*) while not conclusive, the significantly more fluidlike behavior of the leading edge supports the idea that intracellular pressure may be the origin of motive force in neutrophil locomotion.

structural damping; power law; viscoelasticity; optical trap

MECHANICAL DEFORMATION OF LEUKOCYTES, and neutrophils in particular, is an essential feature associated with their function. Examples from the inflammatory response include chemotactically induced locomotion as well as transendothelial and transepithelial migration (21). The mechanical forces responsible for pseudopodial protrusion during locomotion and the cell's resistance to deformation remain controversial. In particular, whether the origin of the protrusive force in pseudopods is causally associated with pushing from polymerizing microfilaments and/or cytoskeletal swelling forces (2, 10, 18, 26), whether it is associated with Brownian ratchets (16), and whether it is the result of hydrostatic pressure with associated fluid flow of cytoplasm into the pseudopod (13, 24) remain open questions. Probes of the rheological properties of cells are an appropriate tool with which to address these issues.

We previously measured intracellular elastic and dissipative properties in neutrophils from 0.3 to 3 Hz by oscillating intracellular granules trapped with optical tweezers, and we interpreted the results in terms of a viscoelastic body (23). Because of this narrow frequency range, it was not possible to determine whether the elastic properties of the cell were independent of the dissipative properties or whether the two were intrinsically coupled. Recent reports (7–9) have strongly suggested that the elastic and dissipative components arise from the same underlying molecular mechanism and are therefore necessarily coupled. This requires measurement of the rheological properties over a significant frequency range. In this article, we report displacement measurements of optically trapped granules after a step change in trap position, which in principle contains all frequencies in the response function. In this manner, we were able to extend our previous frequency range to about three decades (~0.3–500 Hz). We characterized our measurements in terms of simple viscoelasticity and the structural damping model, as recently applied to a variety of cell types, in which stress relaxation is associated with a power law in time (7). These measurements were taken separately in the leading edge, body, and trailing region of locomoting neutrophils to assess regional differences in intracellular rheology. To determine the contribution of the cytoskeletal polymers actin and microtubules, we also measured regional rheology after treatment of the neutrophils with the cytoskeletal disruptors cytochalasin D (actin filaments) and nocodazole (microtubules).

METHODS

Reagents. Krebs-Ringer phosphate with dextrose (KRPD) was constituted as (in mM) 115 NaCl, 14 dextrose, 6 KCl, 4.6 $MgSO_47H_2O$, 3.5 $NaH_2PO_42H_2O$, and 16 Na_2HPO_4 in water. We used normosmotic RPMI 1640 medium with L-glutamine (GIBCO-BRL, Grand Island, NY). For separation of blood cells into mononuclear and polymorphonuclear (PMN) leukocytes, we used Mono-Poly resolving medium (Dainippon Pharmaceutical, Osaka, Japan). Fetal bovine serum was obtained from Cansera International (Etobicoke, ON, Canada). The cytoskeletal disruptors used were cytochalasin D and nocodazole (Sigma Chemical, St. Louis, MO).

Preparation of cells. Human neutrophils were isolated from whole blood by using a density gradient technique described in detail in Yanai et al. (23). Briefly, 24 ml of peripheral blood were drawn from healthy volunteers with a heparinized syringe. Platelets were removed and replaced by KRPD solution, Mono-Poly resolving medium was

Address for reprint requests and other correspondence: M. Yanai, Dept. of Geriatric and Respiratory Medicine, Tohoku Univ. School of Medicine, 1-1 Seiryo-machi, Sendai 980-8574, Japan (E-mail: dept@geriat.med.tohoku.ac.jp).

The costs of publication of this article were defrayed in part by the payment of page charges. The article must therefore be hereby marked "*advertisement*" in accordance with 18 U.S.C. Section 1734 solely to indicate this fact.

 0363-6143/04 $5.00 Copyright © 2004 the American Physiological Society

added, and samples were centrifuged. This procedure resulted in four layers comprising, in order from top to bottom, KRPD solution, a monocyte/lymphocyte layer, a PMN cell layer, and a red cell layer. The PMN cell layer was collected and rinsed with KRPD solution. It was then centrifuged, and the PMN cells were resuspended with 10 ml of medium (RPMI 1640–5% fetal bovine serum).

Chamber preparation. A chamber was prepared with a clean, uncoated slide glass as the top surface and a clean, uncoated coverslip as the bottom surface, separated by ~20 μm using thin plastic sheet spacers. Neutrophils suspended in the medium were introduced into the chamber, the sheet spacers were removed, and the chamber edge was sealed with nail polish. The sample was placed on a microscope stage and maintained at room temperature. Many of the cells remained only loosely adherent to the glass surface and appeared round and inactivated. A modest fraction adhered to the glass strongly and began to spread and locomote. Neutrophils in the process of lamellipodial protrusion and locomotion were used for this study.

Inhibition of F-actin formation and microtubule assembly. To disrupt F-actin or microtubules, we introduced, respectively, cytochalasin D (2 μM) or nocodazole (10 μM) into the chamber in medium containing 0.1% DMSO. The sample was then incubated at 37°C for 5 or 10 min, respectively.

Optical trap and displacement detection. An inverted microscope (IX-70 Olympus) and other optical instruments were set on a vibration-free table (TDI-189LA; HERZ, Yokohama, Japan) as described previously with some modifications (12, 14). As shown in Fig. 1, an intracellular granule in the neutrophil was trapped by an infrared

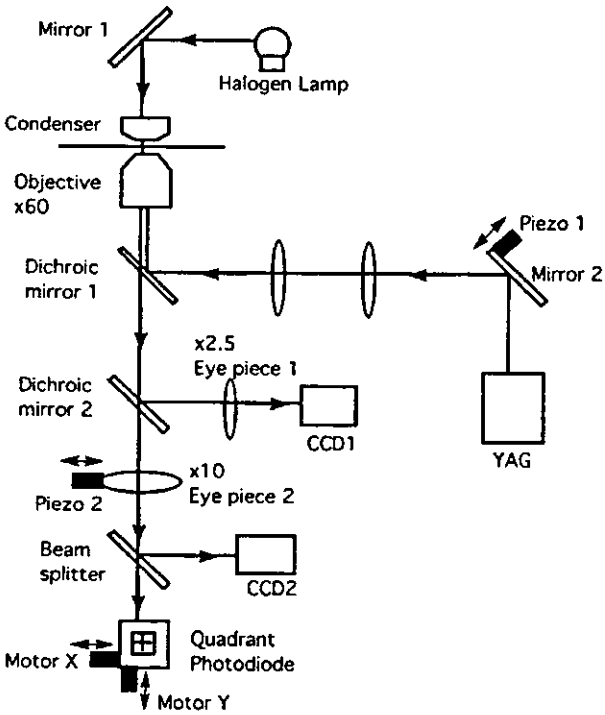

Fig. 1. Schematic of the experimental setup, showing the optical paths involved. These are arranged with three main purposes: *1*) the yttrium-aluminum-garnet (YAG) laser trap's position can be moved (piezo 1, mirror 2), *2*) the motion of a granule is measured by projecting its image in the microscope onto the quadrant photodiode detector, and *3*) the quad detector itself can be moved (motor X or Y) for self-calibration steps during each experimental run. CCD1, charge-coupled device 1; CCD2, charge-coupled device 2.

yttrium-aluminum-garnet laser beam (1,064 nm, 2 W; Spectra-Physics), the position of which was controlled by mirror 2. The images of the neutrophil and enlarged intracellular granule illuminated by a halogen lamp were projected on charge-coupled device cameras 1 and 2, respectively. The center of the granule was projected on the center of a quadrant photodiode detector (1-mm diameter, S1557–01; Hamamatsu Photonics). Displacements of the granule in orthogonal directions were determined from the differential outputs of the detector (differential amplifier OP711A; Sentech, Japan). The stiffness, or equivalent spring constant k_{trap} of the optical trap, was determined from the granular Brownian motion using the equipartition law (19), $k_{trap} \langle x^2 \rangle = k_B T$, where $\langle x^2 \rangle$ is mean square displacements of trapped vesicles, k_B is the Boltzmann constant (1.38×10^{-23} J/K), and T is absolute temperature 300°K. In the present work, the trap stiffness was 0.068 ± 0.018 pN/nm (mean ± SD, $n = 37$). Note that this calibration was done with intracellular granules because the optical properties of the intracellular milieu are different from those of the extracellular medium, and therefore the trap stiffness is different as well.

The position of center of trapping was moved quickly by changing the angle of mirror 2 by means of piezo actuator 1 (see Fig. 1). The 100-nm calibration of the granule displacements was accomplished by moving eyepiece 2 by means of piezo actuator 2. Data of displacement of the granules and the input voltage of piezo 1 and 2 were collected with a computer equipped with a laboratory interface (PowerLab; ADInstruments).

Protocol. A locomoting neutrophil was selected, and a granule in the leading edge, the body, or the trailing region of the cell was optically trapped. An example of granule selection in each region is shown in Fig. 2. This was followed by the step displacement protocol, in which each complete period lasted 2 s. At the beginning of each period ($t = 0$), the trap's position was given a 100-nm step in position, driven by the mirror (piezo 1, mirror 2 in Fig. 1) (95% rise time, <1 ms), and held there for 1 s (Fig. 3, *top left*). During the period in which the step is on, the quad detector is moved the equivalent of 100 nm and then back again (motor X in Fig. 1), from $t = 750$ ms to $t = 900$ ms, measured from the beginning of the step. This allows essentially real-time self-calibration of the displacement signal against the known quad detector step. The trap's position is then returned to baseline for 1 s. This cycle is automatically repeated.

Theory. Visual inspection of the displacement data revealed a common feature in all measurements. After the step change in position of the optical trap, there was a very fast rise in the displacement response, although definitely not a step jump in position. This was followed by a much slower approach to a limiting behavior in displacement, which approximated a gently rising plateau. This suggested two potential models to characterize the data. First, the initial large and subsequent decreasing velocity of the granule, together with the presence of an approximate plateau asymptote, suggested consideration of the simplest possible linear viscoelastic description, consisting of an elastic element with stiffness G in parallel with a viscous element with viscosity μ. The advantage of such a description is its simplicity. Second, we modeled the cytoplasmic milieu with the structural damping idea, which is known to characterize a variety of biological tissues and cells (8, 9, 11). [Non-Newtonian fluid characterizations of cell rheology, which share features with structural damping, have also been investigated (5, 20).] In pure structural damping, stress relaxation after a displacement step behaves as a power law in time and is parameterized by an overall scale of stress and the exponent in the power law. Note that both Voigt viscoelasticity and structural damping are two-parameter models.

Both of these models are simple to implement when measurements of force are made after step displacements or when measurements of displacements are made after step changes in force. However, when the position of the trap is a step function, the trapping force applied to the granule is more complicated because the trap's force on the

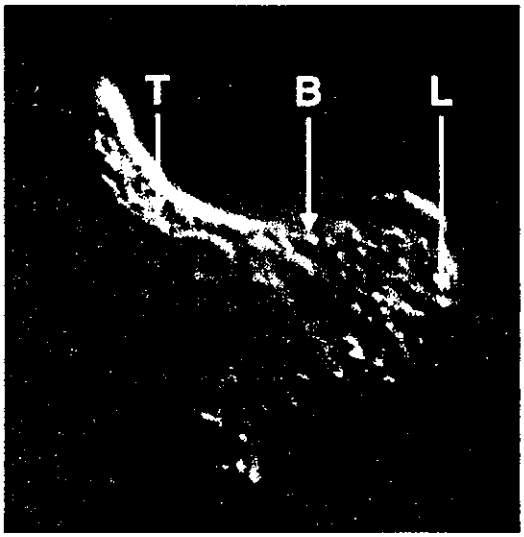

Fig. 2. Differential interference contrast image of a locomoting neutrophil, with arrows denoting granules located at each of the three regions of interest. L, leading edge; B, body; T, trailing region. Scale bar, 4 μm.

granule and the granule's position are coupled (i.e., as the granule moves in response to the trap's force, the force also falls because of the granule's position moving closer to the trap's center). In the case of the simple viscoelastic model, this presents no difficulty, because the force on the granule remains proportional to its displacement. The equations of motion and their solution are described in the APPENDIX. By contrast, the equations of motion are quite complex for a granule in a structural damping medium after a step change in the optical trap's position. The equations of motion and their solution for this case are also provided in the APPENDIX.

All measures of stiffness and viscosity scale with the trap stiffness, which, as determined above, has dimensions of a spring constant, i.e., force/length. This yields essentially one-dimensional stiffness and viscosity measures in characterizing the step response data. As described at the end of the Appendix, it is easy to convert these measures to the more usual elastic moduli and viscosity by using the Stokes formulation for the displacement or velocity of a spherical particle in an elastic or viscous medium. This factor depends only on the particle radius, for which we take a typical granular radius of 300 nm.

All fits to the data were done by least-squares fitting of the measured $x(t)$ against the formulas in *Eqs. A2* (viscoelastic model) and *A10* (structural damping model). This was done for the first 500 ms of data collection (the trap step-on position). Data for times after 1 s, when the trap returned to the origin, were not used because of the confounding effects due to the presence of cellular motion. That is, the model assumptions include stasis of the intracellular milieu, which is variably valid for time scales longer than, in our case, ~1 s. We did choose data runs in which the return transient showed at least an approximate return to the origin, but it was clear that, because of

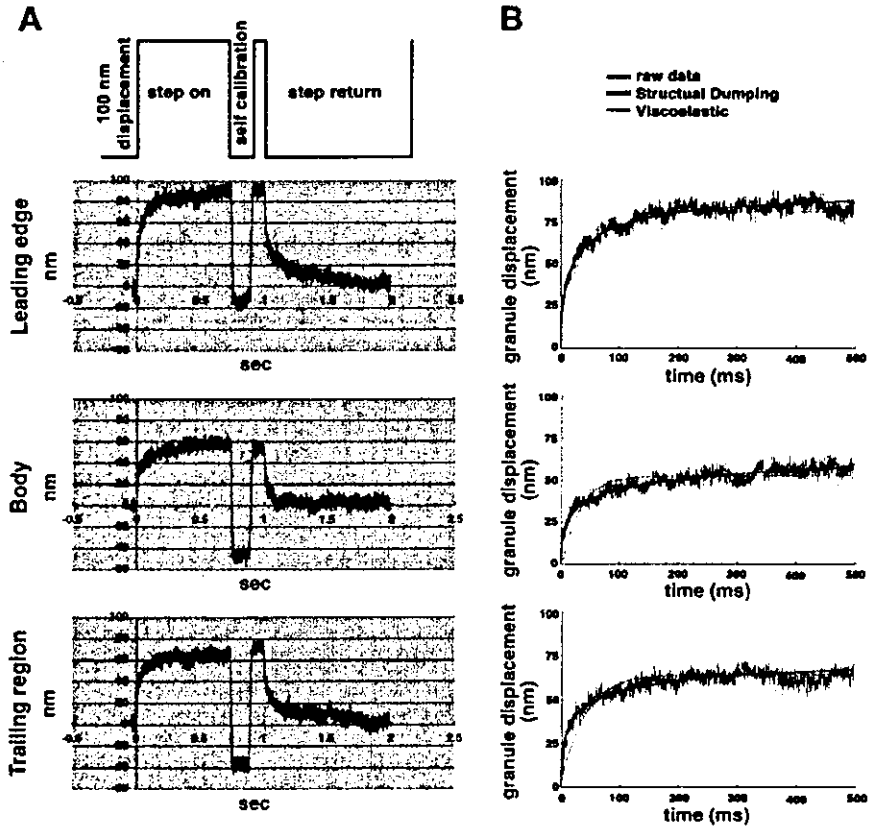

Fig. 3. *A*: schematic of the trap position as a function of time (note the self-calibration jump step and the return to baseline over the 2-s protocol) and three raw data tracings from granular displacement responses in the leading edge, body, and trailing region of a normal locomoting neutrophil. *B*: segments of data analyzed, with fits to the viscoelastic model (shaded traces) and to the structural damping model (solid lines).

locomotion, the reliability of data recorded past 1 s was questionable. The models were compared by examination of the sum of squared residuals. We compared the stiffness and viscosity (viscoelastic model) and stiffness and power law exponent (structural damping model) between the body, trailing, and leading edge of the locomoting neutrophils, and between control conditions and after cytoskeletal disruption, with cytochalasin D (actin filaments) or with nocodazole (microtubules). All data are expressed as means ± SE. Comparisons were done by *t*-test, with significance set at either $P < 0.05$ or $P < 0.01$, as shown in the figures.

RESULTS

A total of 52 cells were studied under control conditions, with 20, 17, and 15 measurements in body, tail, and leading edges of the cell, respectively. Because we found no significant differences between the body and tail regions, these data were subsequently pooled. Body regions were studied in 29 cells after treatment with cytochalasin D; because there was no locomotory activity, there are no data for any leading edge in this treatment group. Pooled body and trailing regions and leading edge regions were studied in 16 and 9 cells, respectively, after treatment with nocodazole.

The three data panels in Fig. 3*A* show typical granular displacement curves vs. time after a step change in the position of the optical trap. These data are from a normal control neutrophil, with the granule located in the leading edge, body, or trailing region, respectively, in the three panels. Note the 150-ms self-calibration step that occurs at 0.75 s. The adjacent panels in Fig. 3*B* show the data segments analyzed, together with the curves fitted to the viscoelastic model and to the structural damping model. Note the shape differences: the body and trailing regions appear stiffer (less granular displacement for the same trap displacement) and more solidlike (generally faster response). Curves from cells treated with nocodazole showed patterns qualitatively similar to these. As noted above, treatment with cytochalasin D completely inhibited any leading edge, and motility was stopped. We thus have no data for the leading edge in cytochalasin D-treated cells; data from the body and trailing regions of these treated cells were similar to data from these regions, shown in Fig. 3.

Figure 4 shows the results of the analysis of control neutrophil rheology as a function of cell region. Figure 4*A* corresponds to the simple viscoelastic model, and Fig. 4*B* corresponds to structural damping. In both models, there was no significant difference in any parameter between the body and trailing region of the cell. These regions were therefore pooled for later analysis and for comparison with the rheology after pharmacological intervention. By contrast, both measures of stiffness (G in the viscoelastic model and the stress scale F_{100ms} in structural damping) in the leading edge were significantly lower. Similarly, both measures of fluidity (the viscosity μ in the viscoelastic model and the power law exponent in structural damping) were significantly different in the leading edge compared with the body or trailing region. Both measures (lower μ, higher k) support the idea of a more fluidlike characteristic of the cytoplasm in the leading edge.

With cytochalasin D treatment, we found that the cells were virtually stationary; because there was no locomotion, there was no leading edge. Comparisons were therefore made between the cytochalasin D-treated cells and the pooled body and trailing regions of control cells. Disruption of microtubules

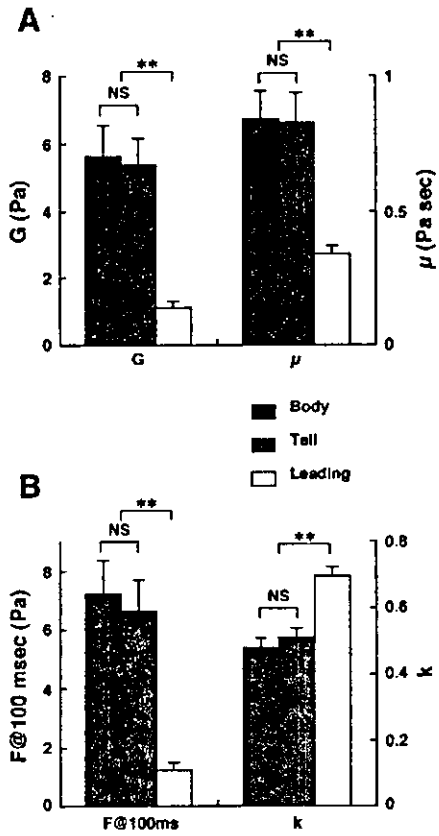

Fig. 4. Rheology of control neutrophils distinguished by cell region. *A*: elastic modulus G and viscosity μ in a simple viscoelastic model. *B*: structural damping stiffness F scaled to 100 ms and power law exponent k in the structural damping model. $^{**}P < 0.01$. NS, not significant.

with nocodazole did not prevent locomotion; in this case, comparisons were possible against both the pooled body and trailing regions of control cells, as well as against the leading region. These results are shown in Fig. 5. Fig. 5, *A* and *B*, shows the viscoelastic stiffness and viscosity in control conditions and after treatment. Figure 5, *C* and *D*, shows the structural damping stiffness and power law exponent in control conditions and after treatment. Figure 6 shows the results displayed as %change from control conditions, with Fig. 6*A* showing the viscoelastic parameters and Fig. 6*B* showing the structural damping parameters. We found that in the body and trailing regions, with either cytochalasin D or nocodazole treatment, the stiffness of the cell as assessed in both models was significantly reduced. Similarly, both treatments reduced the apparent viscosity in the pooled body and trailing region. By contrast, disruption of microtubules with nocodazole did not significantly change any parameter in the leading region of the cell. Perhaps most surprisingly, the power law exponent in structural damping was not changed by any treatment in any cellular region.

The sum of squared residuals for the simple viscoelastic model was averaged over all measurements, separately by cell region and by drug treatment. In all cases, we found that the structural damping characterization fit the data better than did

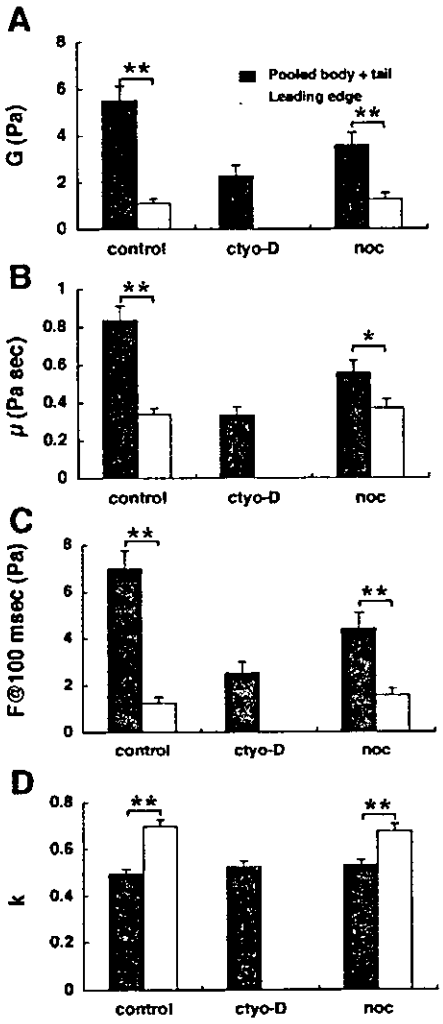

Fig. 5. Rheology of neutrophils in control conditions and after cytoskeleton disruption effected by treatment with cytochalasin D (cyto-D) or nocodazole (noc). From the observation of no significant difference between the body and trailing region of the cell (see Fig. 4), the body and trailing region results were pooled. The neutrophils did not locomote after cytochalasin D, and therefore no data are shown for the leading edge. *A* and *B*: viscoelastic stiffness and viscosity (control and after treatment). *C* and *D*: structural damping stiffness and power law exponent (control and after treatment). $*P < 0.05$. $**P < 0.01$.

the simple viscoelastic model ($P < 0.01$). However, we choose to report the analyses of both methods because, first, classic viscoelastic parameters are easily understood and can be compared with other such common measures in the literature, and second, there is complete agreement between both methods regarding the similarities or significant differences among cell regions and after cytoskeletal disruption.

DISCUSSION

Characterization of rheological properties as simple viscoelasticity. Over a limited frequency range, and when force/displacement Lissajous loops are approximately elliptical, or when a step response is roughly exponential (both being consistent with linearity), a classic description of the phenomena in terms of a simple viscoelastic medium is attractive. In our case, because the approximate displacement plateau that the granule reached after the trap step was systematically less than the trap step size, the standard solid, or Kelvin, model might be considered. On the other hand, we saw no evidence of a sharp jump or step in the displacement, suggesting that the spring constant in the Maxwell body component of the standard solid is very stiff compared with the parallel elastic element. We thus used the simpler parallel viscoelastic model, known as a Voigt body. Such a description is conceptually simple and parsimonious; its two parameters clearly distinguish between energy that can be stored elastically through displacement per se and energy that is dissipated viscously through the rate of change of displacement. On the other hand, as the frequency range over which measurements are made is increased, other behaviors can become apparent, as is the case here; the structural damping model systematically fit the data better than did simple viscoelasticity. Nevertheless, the viscoelastic model remains a useful descriptor. We also investigated other potential models, including a "cage" model of the cytoskeletal network wherein the granules reside in a fluid regime, but as they are displaced, they encounter the cytoskeleton at some particular displacement length. This model is manifestly nonlinear and is not consistent with the approximate

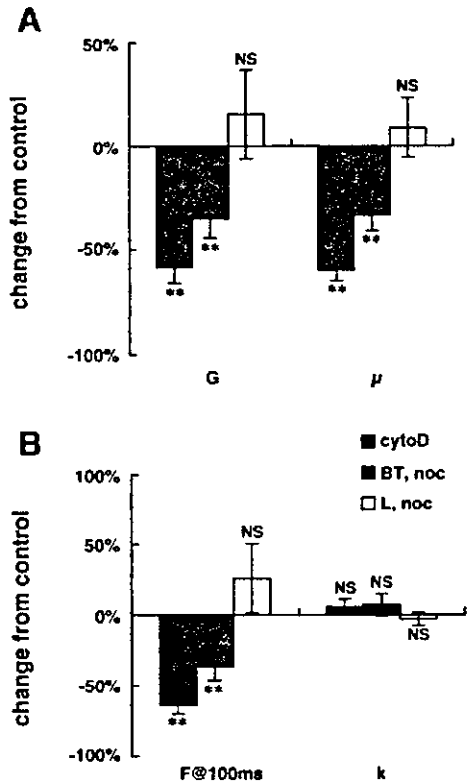

Fig. 6. Percent changes in rheological parameters from control conditions after treatment with either cytochalasin D or nocodazole. *A*: viscoelastic stiffness and viscosity. *B*: structural damping stiffness and power law exponent. $**P < 0.01$. BT, pooled body and trailing regions.

mirror symmetry that we observed when the trap, while still on, returned to the coordinate origin.

Characterization of rheological properties with structural damping. The idea of structural damping arose from the observation, in a number of materials, of a nearly frequency-independent phase of the complex stiffness (or equivalently, a roughly frequency-independent fractionation of stress-bearing properties between those that are recoverable and those that are dissipative). This is an old phenomenological model that has been used successfully in the material science literature for more than a century; it has been applied to biological tissues in the past few decades (e.g., in lung tissue, see Refs. 8, 11; in neutrophils specifically modeled with non-Newtonian fluids that mimic some aspects of structural damping, see Refs. 5, 20). More recently, Fabry et al. (7) found strikingly consistent structural damping in several cell types, including neutrophils, with a variety of pharmacological interventions and over five decades in frequency. The unique feature of structural damping is that stress relaxation follows a power law in time (unlike simple viscoelastic materials, which show exponential behavior). That is, after a unit step displacement, the force falls proportional to t^{-k}. Note that as $k \rightarrow 0$, the material is more elastic (this limit is trivial to verify), and that as $k \rightarrow 1$, the material is more viscous (this limit is more delicate and involves an unbounded apparent stiffness). In this formulation, as noted in the APPENDIX, there is no intrinsic time scale or time constant of the material. To obtain one-dimensional stiffness or elastic modulus with the usual units, one nondimensionalizes time by the introduction of a suitable time scale τ that is determined by the scale of the experiments rather than by the material. The stress relaxation then is written proportional to $(t/\tau)^{-k}$. Our results have been scaled to 100 ms, a convenient choice representative of our experiments.

The numerical value that we found for the structural damping stiffness in the body and trailing region of the cell is ~7 Pa; this is scaled at 100 ms, for which the conversion to ordinary stiffness, given a structural damping exponent of 0.5, corresponds to roughly the same numerical value at 1 Hz. Note that this corresponds to an effective one-dimensional spring constant of ~0.06 pN/nm for a 300-nm radius granule and that therefore a 100-nm displacement implies a net force on the granule of ~6 pN. In our previous work (23), we found neutrophil stiffness on the order of 1 Pa at 1 Hz, but in that study, the granules were separated into fixed and free fractions, with the latter being the only ones in which measurements could be made. The exclusion of the very stiff granules from analysis may account for the almost 1 log increase in stiffness found in this study. It is also the case that the numerical value for stiffness deduced from structural damping measurements depends on the time scale used to nondimensionalize time (see *Eq. A3*). Extrapolations of our data to time scales of, for example, 10 s, reveal stiffness on the order of 0.7 Pa for the body and trailing regions and 0.04 Pa for the leading edge.

Importantly, the stiffness that we found in the leading edge of the cell was roughly 10 times lower, and this is approximately true independent of the time scales used (this ratio increases to almost 20:1 for a 10-s time scale). Using the viscoelastic model, we note that both the stiffness and the viscosity in the leading edge are significantly less than in the body or trailing region but that the stiffness fell more than the viscosity. This is reflected in the equivalent viscoelastic time constant, given by the ratio of the viscosity to the stiffness. In the body and trailing regions, this viscoelastic time constant was ~0.15 s^{-1}, doubling to 0.3 s^{-1} in the leading edge. This is consistent with our interpretation that the leading edge is significantly more fluidlike than the body or trailing region.

Other rheological techniques. Rheological measurements have also been made with micropipette aspiration techniques. Schmid-Schönbein et al. (17) and Chien and Sung (3) reported low-frequency stiffness in the 10- to 15-Pa range, similar to our results. This suggests that the intracellular properties (which we measured directly) are an important contributor to the stiffness as measured by the aspiration technique. These authors used the standard solid model to characterize their data, but it is very interesting to note that, for example, Schmid-Schönbein et al. (see Fig. 7, *A* and *B*, in Ref. 17) reported data that systematically departed from the standard model fit. In particular, their data showed a sharper rise and a slower tail than could be expressed in exponential terms. This is precisely the feature that structural damping exhibits and is fully consistent with our observations.

By contrast, Zahalak et al. (25), using a cell-poking technique, found stiffness in excess of 100 Pa. Again, this technique probes the cell from the plasma membrane and thus displays an average behavior that is necessarily strongly influenced by inhomogeneities of stiffness within the cortical region of the cell. Frequency sweeps using atomic force microscopy have also been done. Recently, Mahaffy et al. (15) measured the microrheology of polymer gels and fibroblasts. While the latter cell type is very stiff compared with neutrophils, we note two very interesting features of their data. First, there is a roughly equal division of stress between those that are elastic and those that are dissipative. This corresponds, in the structural damping theory, to a power exponent of 0.5, which is very similar to what we have found. Second, both these statements are supported by the fact that their stiffness measures show an approximate square root dependence on frequency (stiffness increases of roughly a factor of 2 for a 4-fold frequency increment). We find this to be further evidence of structural damping.

Finally, Yamada et al. (22) used laser-tracking microscopy of intracellular Brownian motion to characterize the mechanics of kidney epithelial COS-7 cells. This work most closely approximates our own insofar as it is a direct intracellular probe (albeit with a completely different cell type). Interestingly, they found elastic moduli to increase slowly with frequency, with a power law exponent slightly less than 0.5. This is further reflected in the approximately constant phase angle that they found, which is somewhat less than the phase angle of $\pi/4$, which would correspond to our power law exponent of 0.5.

The value that we measured for the structural damping exponent, roughly 0.5 for the body and trailing region of the locomoting neutrophil, is similar to the exponent found by Tsai et al. (20) and Drury and Dembo (5) in their investigations of shear thinning of the neutrophilic cytoplasm. However, these are models using the characteristics of pure non-Newtonian fluids without a necessary elastic component, and it is not clear whether this represents a coincidence of exponent in the two approaches or whether it is a deeper manifestation of underlying structure.

It is important to recognize that an exponent of ~0.5 is significantly larger than any of those found by Fabry et al. (7), in differing cell types, and after treatment with contractile and relaxing agonists or with cytoskeletal disruptors. In the specific case of neutrophils, they found an exponent near 0.2 (meaning the neutrophil appeared much more rigid than we found). This large difference in the value of the exponent is interesting and potentially significant. Importantly, the measurements of Fabry et al. (7) were made by observing the lateral displacement of magnetic beads bound to the cell surface through β_2-integrins, for which there is ample evidence that the beads are thereby intimately connected to the cytoskeleton through focal adhesion complexes. But the characteristics of the cytoskeleton that are probed are thus necessarily associated with the cortical region of the cell and with the mechanical properties of the focal adhesion, because that is the immediate locale of all stress-bearing elements. There is no a priori reason to suppose that the rheological properties are uniformly distributed throughout the cell's body, including the cortex and ligated integrin receptors, quite apart from the manifest differences between the leading edge behavior and the rest of the cell. We therefore interpret these different observations as evidence of inhomogeneous properties of the intracellular distribution of the cytoskeleton, with its behavior being much stiffer and more solidlike in the cortical region, especially near focal adhesions, and more dissipative in the interior. This is support for, and perhaps a reconciliation of, different models of cellular rheology, including those that envision an elastic cortical region surrounding a fluid or viscoelastic core (4, 6), which, when probed in the cortical vicinity, would appear more elastic than when probed in the interior.

Implications of leading edge fluidity. Our results strongly suggest that the leading edge of locomoting neutrophils contains a more fluidlike core than either the body or the trailing region. This is important for the identification of the motive force involved in pseudopodial protrusion; its fluidity in turn is consistent with the idea that cytoplasmic flow into the pseudopod is driven by a pressure gradient, although it is not conclusive evidence. While we appreciate that stresses can be borne by either elastic or viscous elements, we do not see how to reconcile polymerizing microfilaments in the advancing pseudopod with significantly increased fluidity. Of course, both F- and G-actin flow into the developing pseudopod, and important polymerization events follow. The presence of increased F-actin near or within the pseudopod, however, does not necessarily imply a role in the initiation or protrusive event itself, as distinguished from subsequent traction and stress-bearing roles that have downstream importance. To the extent that pressure gradients are the origin of pseudopod formation and subsequent cytoplasmic flow (24), some kind of contractile machinery is implied that may be of cortical origin or perhaps even within the entire body of the cell.

Cytoskeletal disruption. Our results with regard to the cytoskeletal disruptors may be interpreted as follows. First, it is clear that disruption of the actin tension-bearing elements with cytochalasin D will lower the apparent stiffness, as will disruption of the microtubules with nocodazole. It is striking that there appears to be an approximately proportional fall in the viscosity (in the viscoelastic model) or, equivalently, that the structural damping exponent k is approximately invariant. These observations are consistent with a coupling at the molecular level of those elements (e.g., actin binding proteins) that may be important contributors to both stiffness and energy dissipation (through bond breakage). In this sense, if the same molecular elements are the origin of both the energy storage and energy-dissipative mechanisms, then it follows that in the absence of other effects, a decrease in their concentration through cytoskeletal disruption will reduce both proportionately. To the extent that the structural damping power law exponent is a function only of the ratio of energy dissipation to energy storage, it is then a proper intensive variable that is independent of concentration. We note that these observations stand in sharp contrast to the work of Fabry et al. (7), who consistently found an increase in the structural damping exponent after treatment with cytochalasin D (i.e., the cell is more fluidlike). It remains unclear why the cell should look more fluidlike after microfilament disruption when viewed from the cell surface and yet retain its basically equal division of elastic and dissipative intracellular properties. Finally, we note that finding little change in any rheological property of the leading region with nocodazole treatment implies little role for microtubules in pseudopodial protrusion.

In summary, we have found that *1*) structural damping is more faithful to observed data than is a viscoelastic parallel spring-dashpot model; *2*) independent of the model, the body and trailing regions of the neutrophil are rheologically indistinguishable; and *3*) also independent of the model, the leading or pseudopodial region is significantly less stiff, less viscous, and more fluidlike than is the body or trailing region. While not conclusive, this is consistent with intracellular pressure being the origin of the motive force that drives pseudopodial protrusion in locomoting neutrophils.

APPENDIX

Here we describe mathematically the displacement of a granule, given a step change in the optical trap position for the viscoelastic and structural damping models of the intracellular milieu.

Viscoelastic model. In this case, the cytoplasm is modeled as a simple viscoelastic medium of stiffness G in parallel with a viscosity μ. The force of the optical trap on the granule at position x is $F = K(a - x)$, where K is the trap stiffness and a is the step displacement in the trap position. Force balance then yields the equation of motion

$$K(a - x) = Gx + \mu dx/dt. \quad (A1)$$

The solution to this problem is elementary:

$$x(t) = \frac{aK}{K + G}(1 - e^{-\beta t}), \quad (A2)$$

where $\beta = (K + G)/\mu$. ($1/\beta$ is the time constant.)

Structural damping. This model rests on a power law behavior of stress adaptation after a step response in displacement:

$$F_{step} = F_\tau(t/\tau)^{-k} \quad (A3)$$

for a unit step in x. The exponent in the power law is restricted to the range $0 < k < 1$. Here F_τ is stiffness (with the usual units of force/length) for a particular choice of time scale τ, typically that of the experimental probe. Note the important point that τ does not represent a time constant of any kind that is characteristic of the medium; it is arbitrary and is conveniently chosen to fall somewhere in the middle of the time scales spanned by the experiments.

The force of the trap on the granule remains $F = K(a - x)$, as in the viscoelastic model. For simplicity, choose K, a, and τ as units of stiffness, length, and time, respectively. Then the trap force is $F = 1 - x$. The restoring force of the medium on the granule is given by a convolution of the impulse response with the displacement. Thus

$$F = F_{impulse} \otimes x = (dF_{step}/dt) \otimes x = 1 - x. \quad (A4)$$

This may be solved in the Laplace domain, denoted by tildes. Thus $s\tilde{F}_{step}\tilde{x} = s^{-1} - \tilde{x}$, or

$$\tilde{x} = s^{-1}(1 - s\tilde{F}_{step})^{-1}. \quad (A5)$$

The Laplace transform of the step response is given by $\tilde{F}_{step} = F_\tau\Gamma(1 - k)s^{k-1}$, where $\Gamma(\cdot)$ is the Legendre Γ function (recall time is nondimensionalized by τ). The solution for the displacement in the Laplace domain is therefore

$$\tilde{x} = \frac{1}{s[1 + F_\tau\Gamma(1 - k)s^k]}. \quad (A6)$$

The time-dependent solution $x(t)$ is given by the inverse Laplace transform of this equation, but unfortunately it does not exist in terms of the elementary transcendental functions. Padé approximations are appropriate in this case (1). In this method, one replaces the desired function with an approximation such that both the short and long time limits (equivalently, the large and small s behavior) are asymptotically matched.

The large s (short t) solution is given by a Taylor series expansion about $s = \infty$:

$$\tilde{x} = s^{-1}\sum_{n=1}(-1)^{n-1}(F_\tau\Gamma(1-k)s^k)^{-n}, \quad (A7)$$

which has the explicit inverse given by

$$x(t) = \sum_{n=1}\frac{(-1)^{n-1}}{\Gamma(1 + nk)}\left(\frac{t^k}{F_\tau\Gamma(1-k)}\right)^n. \quad (A8)$$

This is a convergent series and is exact. Unfortunately, it converges very slowly for large times; it is suitable as written for the short time solution.

For small s (large t), note that the asymptotic limit is $x = 1$; thus we expand $y = 1 - x$, $\tilde{y} = s^{-1} - \tilde{x}$ in a Taylor series about $s = 0$:

$$\tilde{y} = s^{-1} - s^{-1}/(1 + F_\tau\Gamma(1-k)s^k) = F_\tau\Gamma(1 - k)s^{k-1}\sum_{n=0}(-1)^n(F_\tau\Gamma(1 - k)s^k)^n. \quad (A9)$$

The inverse transform of this equation gives the long time behavior, but the series is asymptotic:

$$x(t) = 1 - y(t) = 1 - \sum_{n=1}(-1)^{n-1}\frac{(F_\tau\Gamma(1 - k)t^{-k})^n}{\Gamma(1 - nk)}. \quad (A10)$$

The Padé approximation is constructed as follows. Denote $t^k = u$. Then the behavior near $t = u = 0$ is approximately quadratic: $x(t) = bu + du^2$, where $b = 1/[F_\tau\Gamma(1 - k)\Gamma(1 + k)]$ and $d = -1/[F_\tau^2\Gamma(1 - k)^2\Gamma(1 + 2k)]$. For long times, the solution approaches $x(t) = 1 - F_\tau/u$. We approximate these two behaviors near $t = u = 0$ and $t = u = \infty$ with the Padé rational expression:

$$x(t) = \frac{Bu + Du^2}{1 + Cu + Eu^2}, \; u = t^k, \quad (A11)$$

where $B = b$, $C = (b + dF_\tau)/(1 - F_\tau b)$, and $D = E = d + bC$. This choice of coefficients matches the two-term limiting behavior near both $t = u = 0$ and $t = u = \infty$.

Conversion from one dimension to material moduli. Finally, note that the analyses given above yield stiffness and viscosity values that are one-dimensional in the sense that the stresses are given dimensionally by force/length. To convert these values to the more usual three-dimensional elastic moduli of stiffness (force/area) and viscosity (force·time·area^{-1}), we use the displacement (velocity) of a particle in an elastic (viscous) medium. This yields a constant of proportionality given by $1/6\pi r$, where r is the radius of a typical granule, taken to be 300 nm. This conversion was done for all measurements, except the power law exponent k, which is dimensionless and is not affected by these considerations.

REFERENCES

1. **Bender CM and Orszag SA.** *Advanced Mathematical Methods for Scientists and Engineers.* New York: McGraw-Hill, 1978.
2. **Bottino D, Mogilner A, Roberts T, Stewart M, and Oster G.** How nematode sperm crawl. *J Cell Sci* 115: 367–384, 2002.
3. **Chien S and Sung KL.** Effect of colchicines on viscoelastic properties of neutrophils. *Biophys J* 46: 383–386, 1984.
4. **Dong C, Skalak R, Sung KL, Schmid-Schönbein GW, and Chien S.** Passive deformation analysis of human leukocytes. *J Biomech Eng* 110: 27–36, 1988.
5. **Drury JL and Dembo M.** Aspiration of human neutrophils: effects of shear thinning and cortical dissipation. *Biophys J* 81: 3166–3177, 2001.
6. **Evans E and Yeung A.** Apparent viscosity and cortical tension of blood granulocytes determined by micropipet aspiration. *Biophys J* 56: 151–160, 1989.
7. **Fabry B, Maksym GN, Butler JP, Glogauer M, Navajas D, and Fredberg JJ.** Scaling the microrheology of living cells. *Phys Rev Lett* 87: 148102, 2001.
8. **Fredberg JJ and Stamenovic D.** On the imperfect elasticity of lung tissue. *J Appl Physiol* 67: 2408–2419, 1989.
9. **Gunst SJ and Fredberg JJ.** The first three minutes: smooth muscle contraction, cytoskeletal events, and soft glasses. *J Appl Physiol* 95: 413–425, 2003.
10. **Herant M, Marganski WA, and Dembo M.** The mechanics of neutrophils: synthetic modeling of three experiments. *Biophys J* 84: 3389–3413, 2003.
11. **Hildebrandt J.** Pressure-volume data of cat lung interpreted by a plastoelastic, linear viscoelastic model. *J Appl Physiol* 26: 365–372, 1970.
12. **Ishijima A, Kojima H, Funatsu T, Tokunaga M, Higuchi H, Tanaka H, and Yanagida T.** Simultaneous observation of individual ATPase and mechanical events by a single myosin molecule during interaction with actin. *Cell* 92: 161–171, 1998.
13. **Janson LW and Taylor DL.** In vitro models of tail contraction and cytoplasmic streaming in amoeboid cells. *J Cell Biol* 123: 345–356, 1993.
14. **Kojima H, Muto E, Higuchi H, and Yanagida T.** Mechanics of single kinesin molecules measured by optical trapping nanometry. *Biophys J* 73: 2012–2022, 1997.
15. **Mahaffy RE, Shih CK, MacKintosh FC, and Kas J.** Scanning probe-based frequency-dependent microrheology of polymer gels and biological cells. *Phys Rev Lett* 85: 880–883, 2000.
16. **Peskin CS, Odell GM, and Oster GF.** Cellular motions and thermal fluctuations: the Brownian ratchet. *Biophys J* 65: 316–324, 1993.
17. **Schmid-Schönbein GW, Sung KL, Tozeren H, Skalak R, and Chien S.** Passive mechanical properties of human leukocytes. *Biophys J* 36: 243–256, 1981.
18. **Stossel TP.** On the crawling of animal cells. *Science* 260: 1086–1094, 1993.
19. **Svoboda K, Schmidt CF, Schnapp BJ, and Block SM.** Direct observation of kinesin stepping by optical trapping interferometry. *Nature* 365: 721–727, 1993.
20. **Tsai MA, Frank RS, and Waugh RE.** Passive mechanical behavior of human neutrophils: power-law fluid. *Biophys J* 65: 2078–2088, 1993.
21. **Wagner JG and Roth RA.** Neutrophil migration mechanisms, with an emphasis on the pulmonary vasculature. *Pharmacol Rev* 52: 349–374, 2000.
22. **Yamada S, Wirtz D, and Kuo SC.** Mechanics of living cells measured by laser tracking microrheology. *Biophys J* 78: 1736–1747, 2000.

23. **Yanai M, Butler JP, Suzuki T, Kanda A, Kurachi M, Tashiro H, and Sasaki H.** Intracellular elasticity and viscosity in the body, leading, and trailing regions of locomoting neutrophils. *Am J Physiol Cell Physiol* 277: C432–C440, 1999.

24. **Yanai M, Kenyon CM, Butler JP, Macklem PT, and Kelly SM.** Intracellular pressure is a motive force for cell motion in *Amoeba proteus*. *Cell Motil Cytoskeleton* 33: 22–29, 1996.

25. **Zahalak GI, McConnaughey WB, and Elson EL.** Determination of cellular mechanical properties by cell poking, with an application to leukocytes. *J Biomech Eng* 112: 283–294, 1990.

26. **Zhelev DV, Alteraifi AM, and Hochmuth RM.** F-actin network formation in tethers and in pseudopods stimulated by chemoattractant. *Cell Motil Cytoskeleton* 35: 331–344, 1996.

Biophysical Journal Volume 88 March 2005 2068–2077

Biased Binding of Single Molecules and Continuous Movement of Multiple Molecules of Truncated Single-Headed Kinesin

Takashi Kamei,* Seiji Kakuta,* and Hideo Higuchi*†

*Department of Metallurgy, School of Engineering, Tohoku University, Sendai 980-8579, Japan; and †Center for Interdisciplinary Research and Biomedical and Engineering Research Organization, Tohoku University, Sendai, Miyagi 980-8578, Japan

ABSTRACT Conventional kinesin has a double-headed structure consisting of two motor domains and moves processively along a microtubule using the two heads cooperatively. The movement of single and multiple truncated heads of Drosophila kinesin was measured using a laser trap and nanometer detecting apparatus. Single molecules of single-headed kinesin bound to the microtubules with a 3.5 nm biased displacement toward the plus end of the microtubule. The position of these single-headed kinesin molecules bound to a microtubule did not change until they had dissociated, indicating that single kinesin heads utilize nonprocessive movement processes. Two molecules of single-headed kinesin moved continuously along a microtubule with a lower velocity and force than that of single molecules of double-headed kinesin. The biased binding of the heads determines the directionality of movement, whereas two molecules of single-headed kinesin move continuously without dissociation from a microtubule.

INTRODUCTION

Conventional kinesin is an intracellular vesicle transporter. Kinesin forms homodimers with two motor heads (Bloom et al., 1988; Kuznetsov et al., 1988). The double-headed kinesin moves processively along a microtubule via the cooperative interaction of both heads by utilizing the energy of adenosine 5′-triphosphate (ATP) hydrolysis (Howard et al., 1989). The processivity of single molecules of kinesin ensures high-energy efficiency of vesicle transport and economical protein usage. The unidirectional processive movement has been explained by a hand-over-hand mechanism in which the two heads step alternatively (Asbury et al., 2003; Higuchi et al., 2004; Howard, 2001; Kaseda et al., 2003; Yildiz et al., 2004). It is difficult to distinguish the role of each head during the movement of double-headed kinesin. The movement of each individual head has not been elucidated.

Single-headed conventional kinesin (SHC-kinesin) was genetically constructed using a combination of two previously reported methods (Berliner et al., 1995; Hancock and Howard, 1998). In one method the SHC-kinesin molecules were prepared as monomer heads by truncating the tail section so it did not form the coiled-coil (Berliner et al., 1995). The other method utilized heterodimers by coexpressing full length kinesin with the kinesin tails minus the head portion (Hancock and Howard, 1998). The velocity of the SHC-kinesins was lower than that of double-headed kinesin (Hancock and Howard, 1998; Inoue et al., 2001; Young et al., 1998). The distance the microtubule moved on the SHC-kinesin molecules became shorter as the number of SHC-kinesin molecules interacting with the microtubules in the in vitro motility assay was reduced (Berliner et al., 1995; Hancock and Howard, 1998; Young et al., 1998). This result indicates that the processivity of SHC-kinesin is very low or nonexistent. Hancock and Howard (1998) suggested that 4–6 molecules of SHC-kinesin are needed for continuous movement along a microtubule for distances >300 nm without detachment in an in vitro motility assay. In contrast, Inoue et al. (2001) showed that single molecules of SHC-kinesin move processively along microtubules using a fluorescent imaging technique with video resolution. To clearly show whether single molecules of SHC-kinesin moved processively along a microtubule, recordings at a high spatial resolution were required.

Monomeric motors of the kinesin superfamily, KIF1A or Unc104, provide useful information about the behavior of motor heads of conventional kinesin when interacting with a microtubule, and vice versa. Multiple molecules of KIF1A and Unc104 exhibited continuous rapid movement (Okada et al., 2003; Tomishige et al., 2002). The term 'processive' has been adopted for the movement of individual motor proteins and 'continuous' for the movement of ensembles of motors. Okada and Hirokawa (1999) also showed that single molecules of KIF1A moved processively along a microtubule. Processive movement of KIF1A is enhanced by the electrostatic interaction between the K-loop and the microtubule because the K-loop deleted KIF1A did not move processively beyond the spatial resolution of the image analysis system of ~50 nm (Okada and Hirokawa, 1999, 2000). KIF1A bound to the microtubule moved toward the plus end of the microtubule with a displacement of 2.8 nm (Okada et al., 2003). The direction of the processive movement of KIF1A is determined by the biased binding.

Submitted July 15, 2004, and accepted for publication December 27, 2004.

Address reprint requests to Hideo Higuchi, Center for Interdisciplinary Research, Tohoku University, Aramaki-aza-aoba, Aoba-ku, Sendai, Miyagi 980-8579, Japan, Tel.: 81-22-217-4735; Fax: 81-22-217-7810; E-mail: higuchi@material.tohoku.ac.jp.

Seiji Kakuta's present address is Material Technology Division of Aomori Industrial Research Center, Aomori 030-0113, Japan.

© 2005 by the Biophysical Society

0006-3495/05/03/2068/10 $2.00

doi: 10.1529/biophysj.104.049759

Measuring the displacement of the biased binding of single SHC-kinesin molecules is an important issue to address.

The unidirectional processive movement of single molecules of double-headed kinesin and multiple molecules of monomeric kinesin is an important process used to translocate large vesicles along a microtubule in a cell. To understand the movement of single-headed and double-headed kinesin, we evaluated the movement of single and multiple molecules of SHC-kinesin with nanometer accuracy using a laser trap. Single molecules of SHC-kinesin bound to a microtubule with a definite bias for the plus end of the microtubule and dissociated from a microtubule without exhibiting processive movement. There was no significant displacement of SHC-kinesin molecules bound to the microtubules. Two molecules of SHC-kinesin moved continuously with lower force and velocity than single molecules of double-headed kinesin.

MATERIALS AND METHODS

Protein

SHC-kinesin and double-headed kinesin consist of 351 and 411 amino acid residues from the N-termini of Drosophila kinesin with biotin carboxyl career protein (BCCP) fused at the C-termini. The expression and purification systems have been reported previously by Iwatani and co-workers (Berliner et al., 1995; Huang and Hackney, 1994; Iwatani et al., 1999). Tubulin was purified from porcine brain and the microtubules were labeled with tetramethylrhodamine succinimidyl ester (Molecular Probes, Eugene, OR). The minus end of the microtubules was marked with a higher concentration of rhodamine-labeled tubulin (Howard and Hyman, 1993).

Laser trap nanometry

SHC-kinesin molecules were bound to the polystyrene beads (0.2 μm diameter, Molecular Probes, Eugene, OR) via streptavidin (Sigma, St. Louis, MO; Inoue et al., 1997) and were trapped by an infrared laser (λ = 1064 nm) positioned near a fluorescence-labeled microtubule. Details of the laser trap system and apparatus have been reported previously (Nishiyama et al., 2001; Svovoda et al., 1993). All assays were performed using a solution containing 25 mM K-Acetate, 1 mM EGTA, 4 mM $MgCl_2$, 10 μM Taxol, 0.12 mg/ml casein, and 20 mM K-HEPES (pH 7.2) with an added oxygen scavenger system (0.14 M 2-mercaptoethanol, 20 mM glucose, 20 μg/ml catalase, 100 μg/ml glucose oxydase) at 25°C ± 1°C.

Data analysis

The bead displacements were recorded at a sampling rate of 20 kHz with a bandwidth of 10 kHz. The force produced by SHC-kinesin was calculated from the bead displacement multiplied by the trap stiffness (35 fN/nm) that was determined from the variance of the thermal fluctuations of a trapped bead by the equipartion of thermal theory (Kojima et al., 1997). The velocity, taking into account the attenuation factor, was derived from the low pass filter at 5 Hz. The attenuation factor for correcting the displacement of the SHC-kinesin fragments was evaluated from $(K_t + K_p)/K_p$, where K_t is the stiffness of the optical trap and K_p is that of the bead-to-glass linkage which is the series of linkages of a bead, the SHC-kinesin molecules, a microtubule, and the surface of a glass slide (Kojima et al., 1997; Svoboda et al., 1993). The total stiffness, $K_p + K_t$ of the linkage and the trap, was also calculated from the variance of the bead fluctuations when kinesin interacted with the microtubule.

The displacement at each binding event of single SHC-kinesin molecules to the microtubule was calculated from the displacement multiplied by the attenuation factor. The attenuation factor, 1.72 ± 0.02 (mean ± SE, n = 162), at the displacement of −5 to 5 nm was not a significant difference from 1.69 ± 0.02 (n = 122) at the displacement of −10 to −5 and 5 to 10 nm before attenuation. This factor decreased slightly to 1.62 ± 0.02 (n = 116) at <−10 and >10 nm before attenuation, or <−17 and >17 nm after attenuation.

The velocity of each displacement trace was derived from the slope of the displacement which had been smoothed by a low pass filter of 5 Hz and multiplied by the attenuation factor. The average values of the attenuation factors during continuous movement were 1.7 at low loads of ~1 pN and 1.2 at high loads of >5 pN.

RESULTS

Minimum number of SHC-kinesin molecules required for continuous movement

To make the SHC-kinesin-beads, various concentrations of SHC-kinesin were mixed with a constant concentration of the polystyrene beads, 0.2 μm in diameter, in a solution (~0.01%, v/v or ~60 pM). Beads coated with SHC-kinesin were trapped using optical tweezers and then placed on a microtubule. A reduction in Brownian motion of an SHC-kinesin-bead was considered to be an interaction with a microtubule (Veigel et al., 1999). The ratio of the number of SHC-kinesin-beads interacting with the microtubules to the total number of beads observed at each concentration of SHC-kinesin was determined. Interaction times shorter than 50 ms have not been included to avoid any artifacts resulting from the binding of molecules other than the SHC-kinesin molecules to a microtubule.

In the presence of 1 mM adenosine 5′-(β-γ-imido)triphosphate (AMP-PNP), SHC-kinesin-beads bound to a microtubule for a long time, i.e., for more than several seconds (Fig. 1 *a*). At low concentrations of SHC-kinesin and in the presence of ATP (6 μM), SHC-kinesin-beads bound to and dissociated from a microtubule repeatedly without exhibiting continuous movement (Fig. 1 *b*). Fig. 1, *c* and *d*, shows the continuous movement of SHC-kinesin-beads at high and low ATP concentrations.

In the presence of AMP-PNP, single molecules of SHC-kinesin on the beads should bind to a microtubule for long periods of time because of the strong binding (Endow and Higuchi, 2000; Huang and Hackney, 1994). Thus, the ratio of the interacting beads to the total number of beads indicates the ratio of the beads to which one or more molecules of SHC-kinesin had bound to a microtubule. Assuming SHC-kinesins are distributed randomly on the beads, the number of molecules on the bead can be described by a Poisson distribution (Svoboda and Block, 1994). According to the Poisson distribution, the probability that there are one or more SHC-kinesin molecules on a bead can be described by the curve, $1 - \exp(-C/C_0)$, where C is the concentration of SHC-kinesin (nM) and C_0 is the concentration when the average number of SHC-kinesin molecules on a bead is one (SHC-kinesin concentration of 0.2 nM). The ratio of the beads